Journal of Water Process Engineering

Heterogeneous Fenton-like degradation of organics pollutants in petroleum refinery wastewater by copper-type layered double hydroxides

--Manuscript Draft--

Manuscript Number:	JWPE-D-22-02411R2
Article Type:	Full Length Article
Keywords:	Oil refinery wastewater; hydrotalcite-type; substitution effect; Fenton-like process; Hydroxyl radicals
Corresponding Author:	Ghania RADJI University of Science and Technology of Oran Mohamed Boudiaf Laboratory of Inorganic Materials Chemistry and Applications Oran, ALGERIA
First Author:	Ghania RADJI
Order of Authors:	Ghania RADJI
	Nourredine Bettahar
	Abdellah Bahmani
	Ishak Boukhetache
	Sandra Contreras
Abstract:	A series of Ni (2-x) Cu (x) Al-LDH layered ternary double hydroxides with x:0.0; 0.5; 1.5; and 2.0 were synthesized as catalysts for the degradation of aromatic and aliphatic organic compounds present in petroleum refinery wastewaters by a Fenton-type reaction, using hydrogen peroxide as a free radical generator. Samples obtained by coprecipitation at constant pH with a molar ratio R:(Ni 2+ +Cu 2+)/Al 3+ equal to 2.0 were characterized by PXRD, FT-IR, ESEM-EDS, ICP-OES, TGA and N 2 physisorption. The results of the oxidation reaction showed that the catalytic activity varies inversely with the Ni 2+ /Cu 2+ ratio, and the maximum activity is achieved for x:2.0. This catalyst can remove 74.8% of TOC, where the aromatic compounds could be completely oxidized by H 2 O 2 90 min at 60°C under the conditions of pH:pH IEP and at a less excessive dosage of H 2 O 2 (H 2 O 2 /COD:5), temperature of the reaction medium 60°C, but this catalysis presents other phases than LDH phase, sach as malachite and gibbsite. The catalytic oxidation process had first-order kinetics with an activation energy of 44.803 kJ mol - 1 for the TOC disappearance reaction.
Suggested Reviewers:	
Opposed Reviewers:	
Response to Reviewers:	

HIGHLIGHTS

1. The hydroxyl radicals (•OH) played an important role in the $Ni_{(2-x)}Cu_{(x)}$Al-LDH/H_2O_2 system.
2. Cu^+ is catalytically active in a wide range of pH values.
3. TOC reductions were higher in the presence of Cu^+.

Graphical Abstract

SPRW: Synthetic Petroleum Refinery Wastewater
Toluene + Phenol + Xylene + Naphthalene + o-Cresol + Nonane + Hexadecane

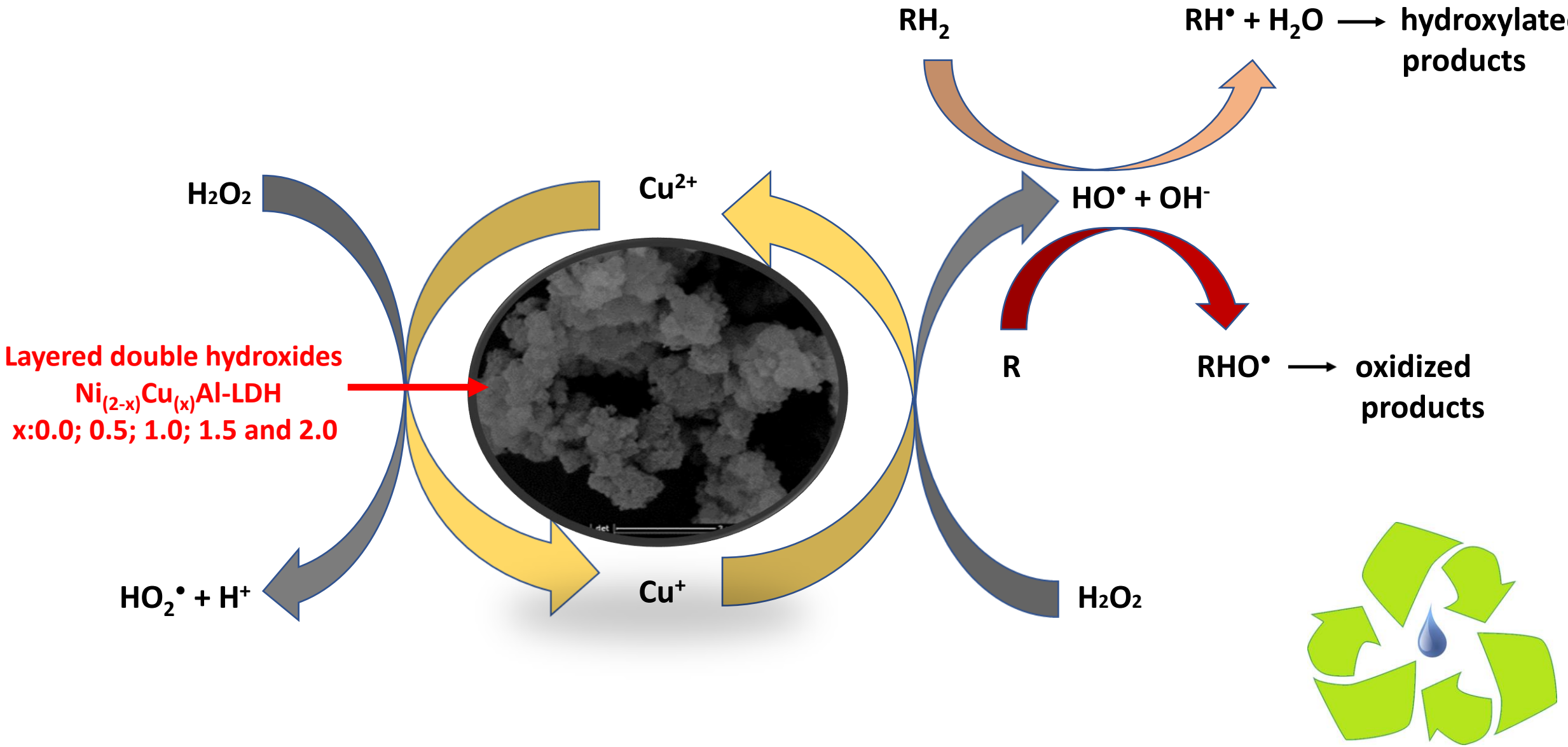

Heterogeneous Fenton-like degradation of organic pollutants in petroleum refinery wastewater by copper-type layered double hydroxides

Ghania Radji,[1, 2 *] Nourredine Bettahar,[1] Abdellah Bahmani,[1] Ishak Boukhetache,[2] Sandra Contreras[3]

[1] *Laboratoire de chimie des matériaux inorganiques et applications (LCMIA). Université des Sciences et de la Technologie d'Oran Mohamed Boudiaf, USTO-MB, BP 1505, El M'naouer, 31000 Oran Algérie*

[2] *Faculté des sciences et de la technologie. Université Ahmed Draia, route nationale N°6, 01000 Adrar Algérie*

[3] *Departament d'Enginyeria Química, Universitat Rovira i Virgili, Av. Països Catalans 26, 43007, Tarragona, Spain*

SUPPLEMENTARY MATERIAL

1. Summary of Experiments Performed within This Study

Table S-1. Mass loss for each temperature range, as well as total mass loss of $Ni_{(2-x)}Cu_{(x)}Al$-LDH catalysts obtained by TGA.

Catalysts	Mass loss (%) [Ambaint-200°C]	Mass loss (%) [200°C-350°C]	Mass loss (%) [350°C-500°C]	Total mass loss (%)
x:0.0	16.0	17.0	4.0	37.0
x:0.5	15.0	18.0	3.5	36.5
x:1.0	14.0	18.0	4.0	36.0
x:1.5	13.0	15.0	5.0	33.0
x:2.0	10.0	17.0	4.0	31.0

Table S-2. The calculated kinetic parameters and activations energy of TOC disappearance rate.

Reaction temperature	k_{app} (min^{-1})	R^2	Ea ($kJ\ mol^{-1}$)
293 K	0.00217	0.95412	44.803
303 K	0.00491	0.94686	
313 K	0.00526	0.95320	
323 K	0.01030	0.98634	
333 K	0.02076	0.96671	
343 K	0.03136	0.96304	
(SPRW, H_2O_2/COD: 5, $Ni_{(2-x)}Cu_{(x)}Al$-LDH with x:1.0: 0.4 g L^{-1}, reaction time: 90 min, pH: pH_{PZC})			

Table S-3. TOC conversion rate obtained (%) for each catalyst.

Catalysts	After 30 min of heating	After 30 min of ads	10 min	20 min	30 min	60 min	90 min
x:0.0	14.65	7.35	0.61	0.83	3.88	6.21	6.23
x:0.5	15.73	6.73	3.99	11.03	12.07	25.57	28.72
x:1.0	15.36	6.04	15.11	25.08	37.77	49.19	65.24
x:1.5	14.53	5.35	18.69	31.00	41.09	53.08	66.95
x:2.0	13.49	4.27	24.29	35.26	46.88	57.66	74.79
(SPRX, H_2O_2/COD: 5, $Ni_{(2-x)}Cu_{(x)}$Al-LDH: 0.4 g L^{-1}, reaction time: 90 min, T: 60°C, pH: pH_{PZC})							

2. Synthesis protocol of catalysts

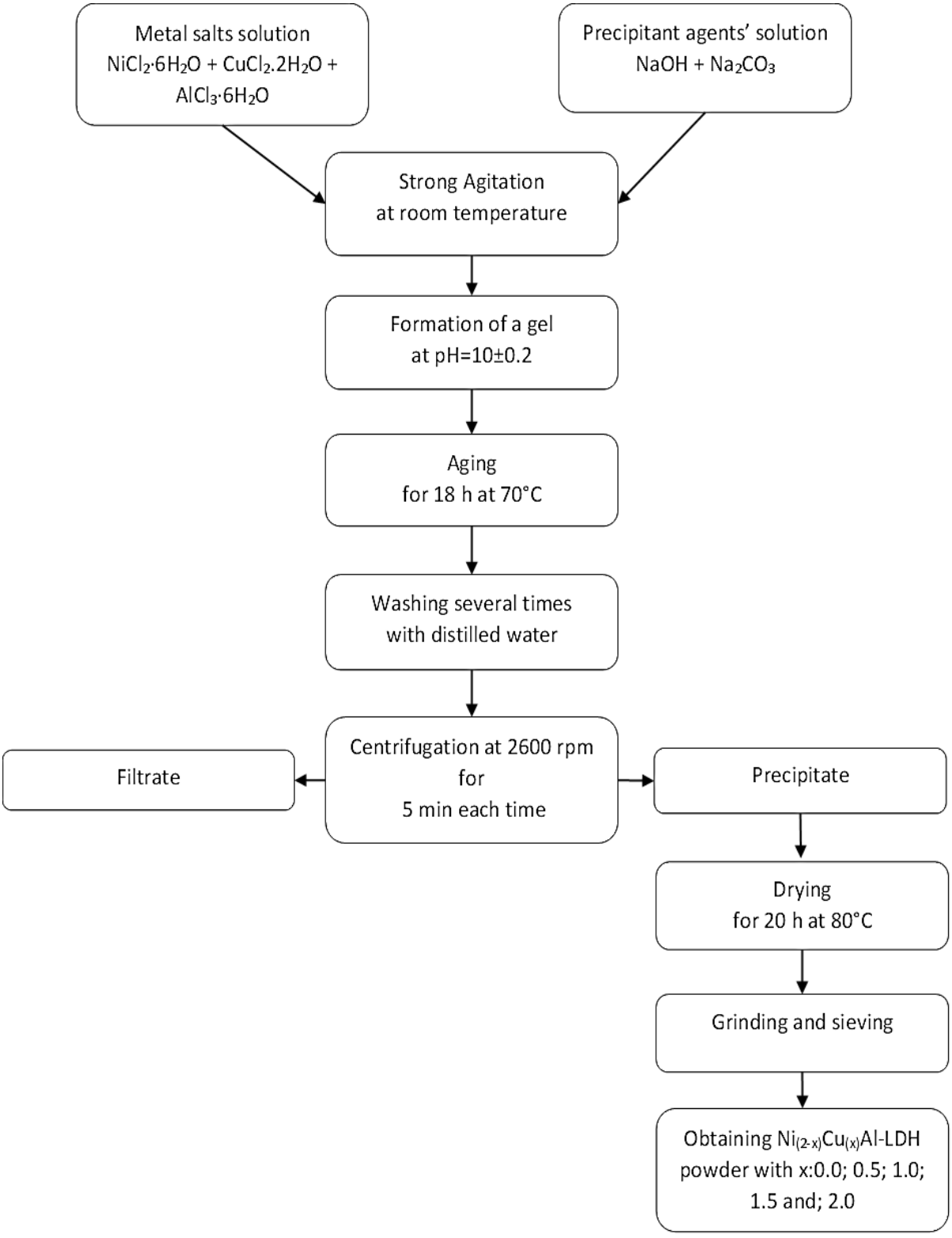

Fig.S-1. Synthesis protocol of $Ni_{(2-x)}Cu_{(x)}Al$-LDH with x:0.0; 0.5; 1.0; 1.5 and 2.0 catalysts

3. HPLC Analyses

HPLC analyses were carried out using a Shimadzu HPLC system equipped with a diode array detector (DAD) and a gradient technique, with the HPLC equipment being supplied by Shimadzu. The mobile phase has been made up of water (which contains 0.1% phosphoric acid) and ACN. The analytes were separated using a Mediterranea HPLC column (C18, 2.1 x 150 mm, 3.5 m, Teknokroma, USA) at a temperature of 40°C. The wavelength of the DAD was fixed at 254 nm. Multiple HPLC gradients were evaluated to ensure adequate peak separation and resolution. By comparing the resulting chromatograms, it was determined that the following gradient program was best for mobile phase flow: Following sample injection, the percentage of ACN was increased linearly from 0 to 10% in a time interval of 0 to 15 minutes; it was then maintained at 25% in a time interval of 15 to 17 minutes, at 80% in a time interval of 17 to 27 minutes, reaching 100% ACN at 27 minutes, and then reduced to 10% over a 32 minutes period. A 7 minutes post-run interval of 10% ACN was established prior to the start of the next sample injection in order to establish a steady state in the separation system and to allow for column regeneration.

4. Extraction Procedure and Conditions for GC-MS Analyses

Before GC-MS analysis, the samples were extracted with dichloromethane (DCM); 50 mL of sample was put to the separatory funnel, along with 10 mL of dichloromethane as the extraction solvent. The mixture was agitated vigorously for 5 minutes and then allowed to settle. The method was repeated twice more (Trouvé et al., 2021). The whole organic phase was analyzed directly by GC-MS using a SHIMADZU GCMS-QP2020 instrument equipped with a fused Rxi®-5ms capillary column (Phase: Crossbond® 5% diphenyl/ 95% dimethyl polysiloxane); its dimensions are 30 m 0.25 mm and its film thickness is 0.25 m. A solution was made by diluting 10% vol of the sample in dichloromethane and injecting 0.5L of the resulting solution in split mode (1:1). The column temperature was planned to be fixed at 40°C for 3 minutes, then escalated to 220°C at a rate of 25°C/min for 10 minutes. Temperatures of the injector and detector were maintained at 250°C and 220°C, respectively. Helium (99.99%) was employed as the carrier gas at a flow rate of 1 mL/min. The mass spectrometer was operated under the following conditions: 200°C ion source temperature, 70 eV ionization voltage, and electron ionization mass spectra were collected in the mass range 40-300 m/z. The series of n-alkanes employed in these investigations was (n-C7-C33).

5. Chromatograms Obtained by HPLC and GC-MS Analyses

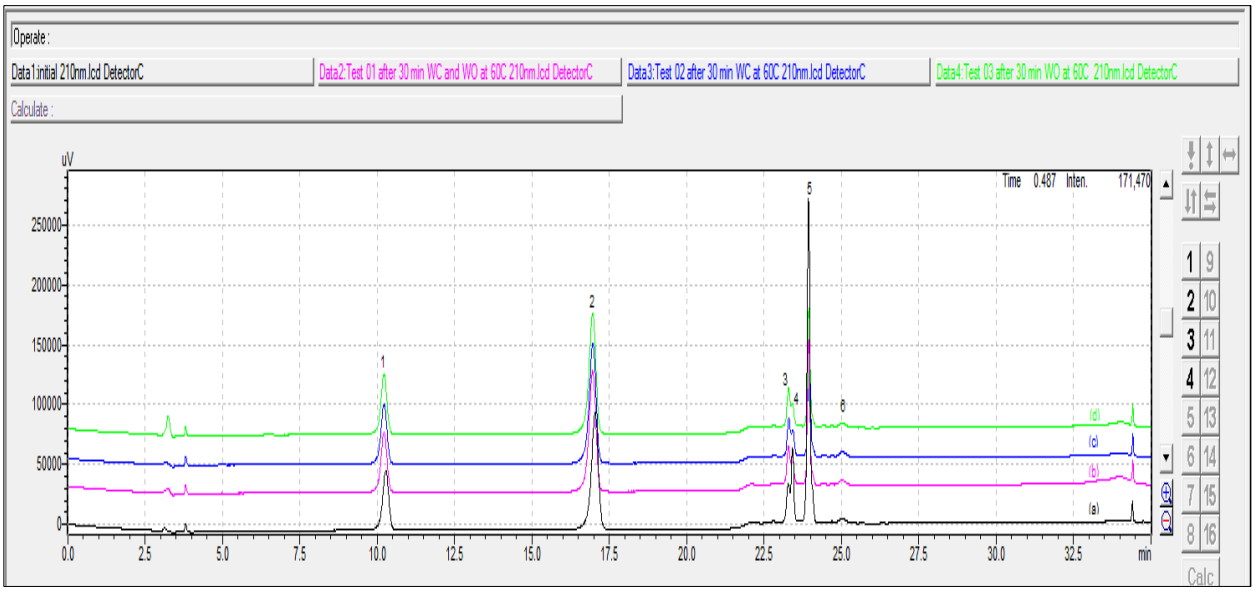

Fig.S-2. HPLC chromatograms (a) Initial SPRW; (b) without catalyst and without oxidant; (c) without catalyst and with oxidant (d) without oxidant and with catalyst (SPRW, H_2O_2/COD: 5, $Ni_{(2-x)}Cu_{(x)}Al$-LDH with x:1.0: 1.0 g L^{-1}, T: 60°C, reaction time: 30 min, pH: pH_{PZC})
1) Phenol; 2) O-Cresol; 3) Toluene; 4) Naphthalene; 5) Xylene and 6) Titon X-100

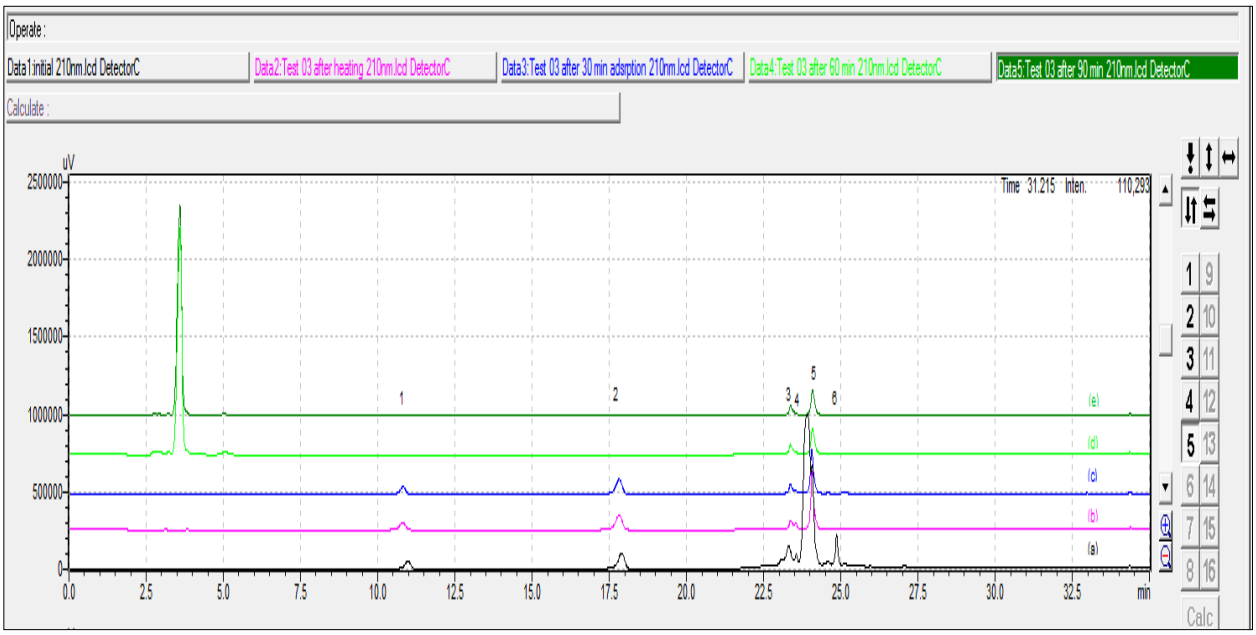

Fig.S-3. HPLC chromatograms (a) Initial SPRW; (b) After 30 min heating; (c) After 30 min adsorption; (d) After 60 min of reaction and (e) After 90 min of reaction (SPRW, H_2O_2/COD: 5, $Ni_{(2-x)}Cu_{(x)}Al$-LDH with x:1.0: 1.0 g L^{-1}, T: 60°C, reaction time: 90 min, pH: pH_{PZC})
1) Phenol; 2) O-Cresol; 3) Toluene; 4) Naphthalene; 5) Xylene and 6) Titon X-100

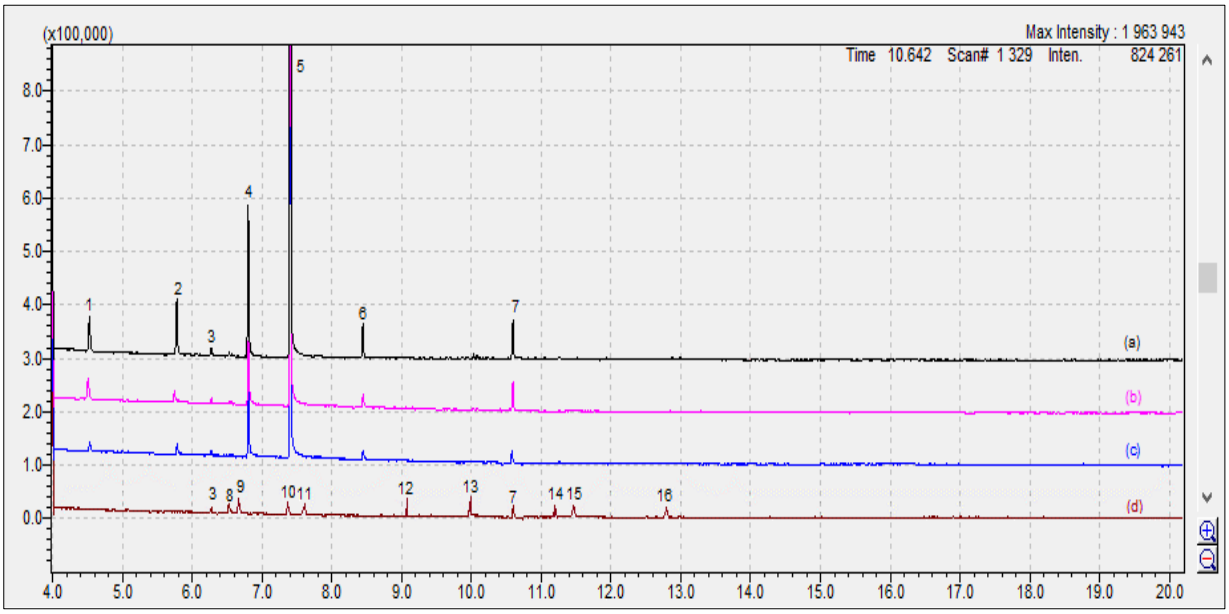

Fig.S-4. GC-MS chromatograms (a) Initial SPRW; (b) After 30 min heating; (c) After 30 min adsorption and (d) After 90 min of reaction (SPRW, H_2O_2/COD: 5, $Ni_{(2-x)}Cu_{(x)}Al$-LDH with x:1.0: 1.0 g L^{-1}, T: 60°C, reaction time: 90 min, pH: pH_{PZC})
1) Toluene; 2) Xylene; 3) Nonane; 4) Phenol; 5) O-Cresol; 6) Naphthalene; 7) Hexadecane, 8,9) Organics acids and 10-16) Alkanes

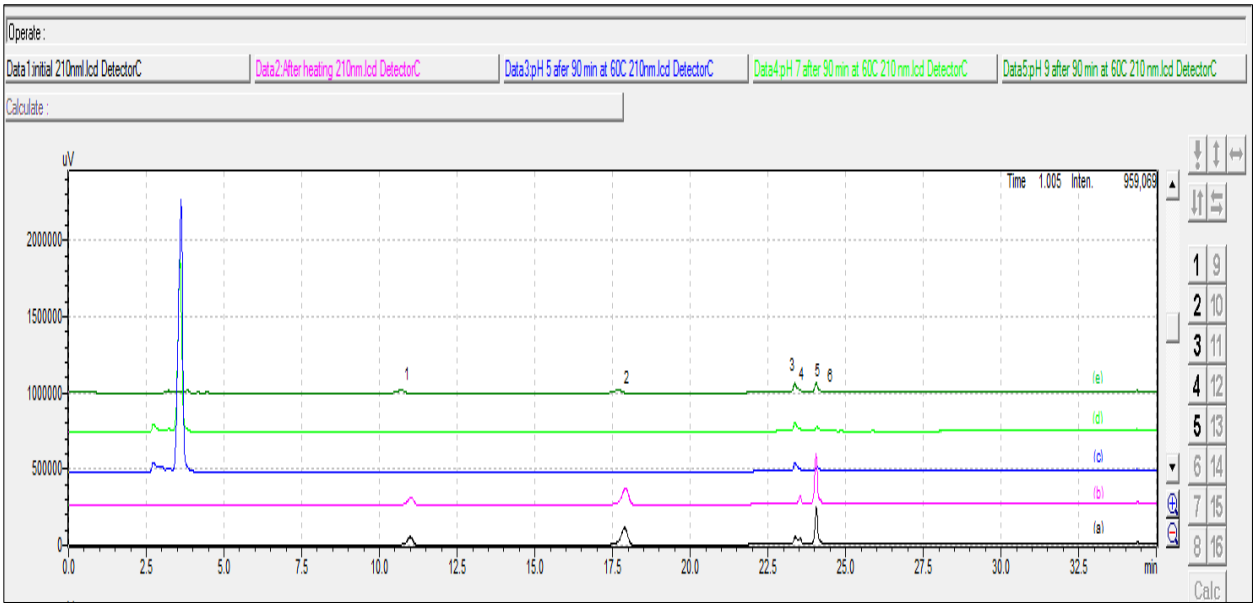

Fig.S-5. HPLC chromatograms (a) Initial SPRW; (b) After 30 min heating; (c) At pH 5; (d) At pH 7 and (e) At pH 9 (SPRW, H_2O_2/COD: 5, $Ni_{(2-x)}Cu_{(x)}Al$-LDH with x:1.0: 0.4 g L^{-1}, T: 60°C, reaction time: 90 min)
1) Phenol; 2) O-Cresol; 3) Toluene; 4) Naphthalene; 5) Xylene and 6) Titon X-100

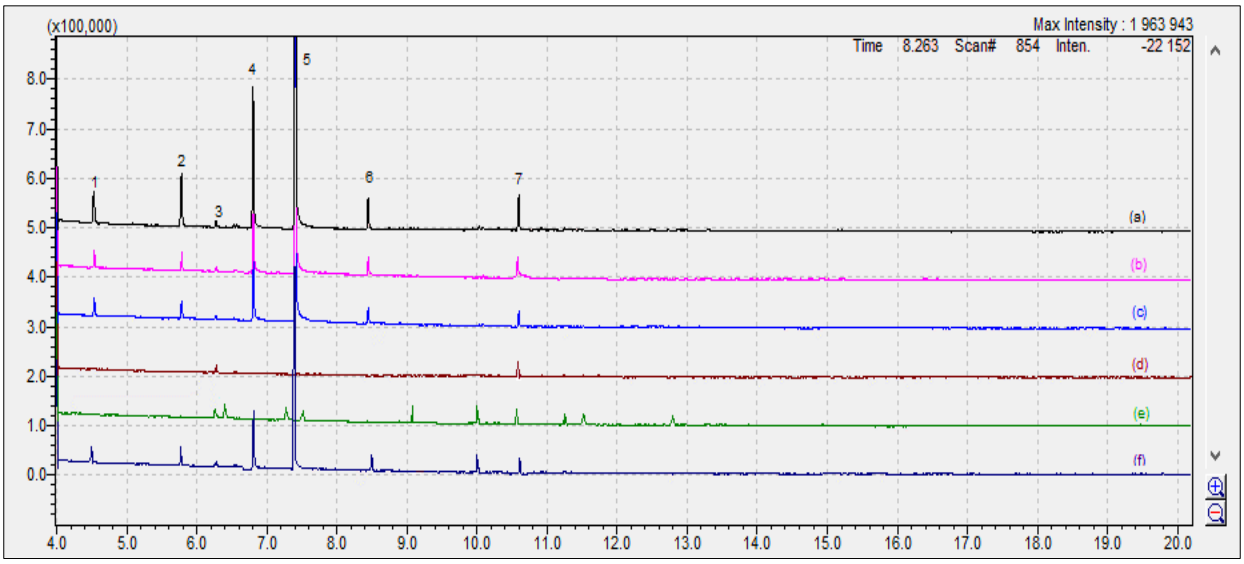

Fig.S-6. GC-MS chromatograms (a) Initial SPRW; (b) After 30 min heating; (c) After 30 min adsorption; (d) At pH 5; (e) At pH 7 and (f) At pH 9 (SPRW, H_2O_2/COD: 5, $Ni_{(2-x)}Cu_{(x)}$Al-LDH with x:1.0: 0.4 g L^{-1}, T: 60°C, reaction time: 90 min)

1) Toluene; 2) Xylene; 3) Nonane; 4) Phenol; 5) O-Cresol; 6) Naphthalene; 7) Hexadecane

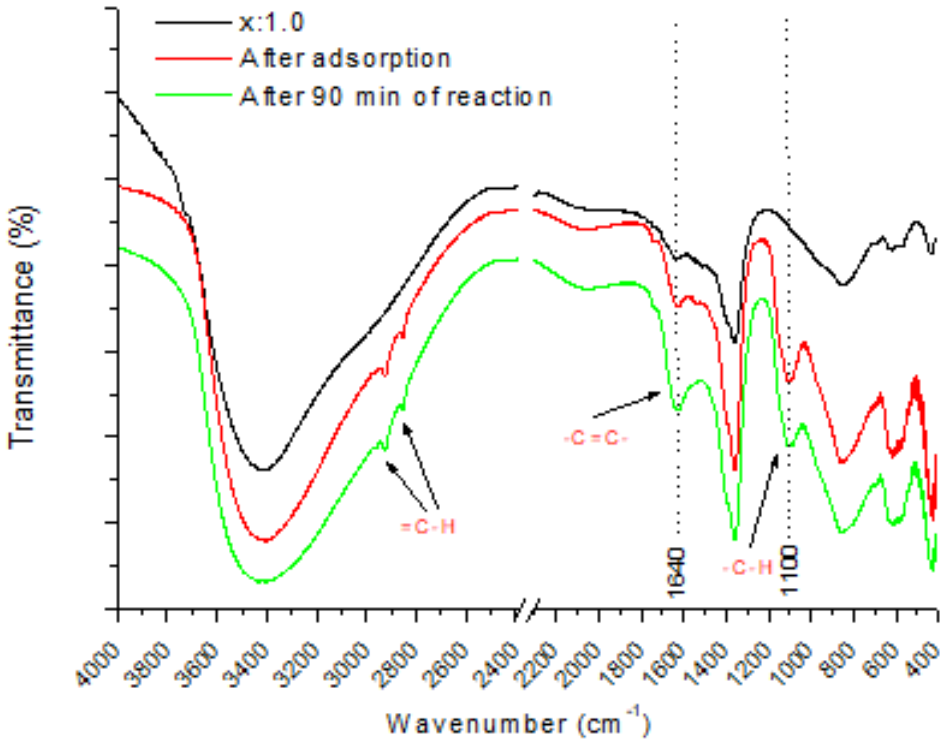

Fig.S-7. FT-IR spectra of $Ni_{(2-x)}Cu_{(x)}$Al-LDH with x:1.0; after 30 min of adsorption and after 90 min of reaction

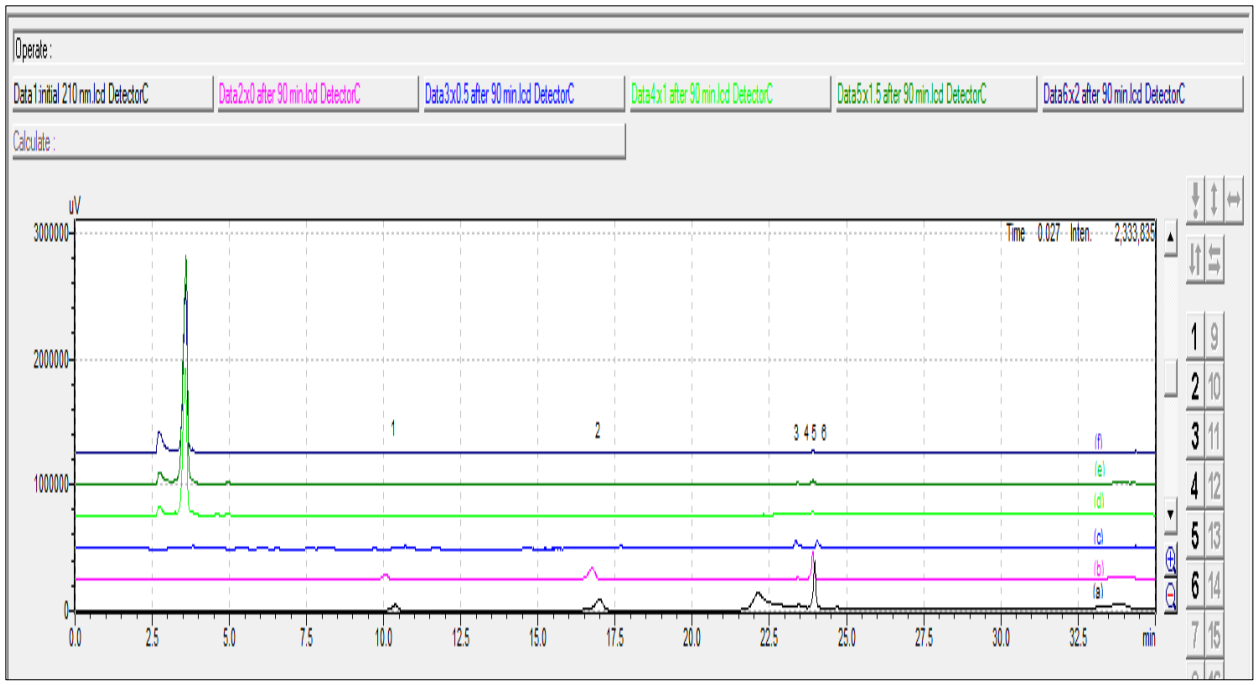

Fig.S-8. HPLC chromatograms (a) Initial SPRW; (b) x:0.0; (c) x:0.5; (d) x:1.0 (e) x:1.5 and (f) x:2.0
(SPRW, H_2O_2/COD: 5, $Ni_{(2-x)}Cu_{(x)}$Al-LDH: 0.4 g L^{-1},
T: 60°C, reaction time: 90 min, pH: pH_{PZC})
1) Phenol; 2) O-Cresol; 3) Toluene; 4) Naphthalene; 5) Xylene and 6) Titon X-100

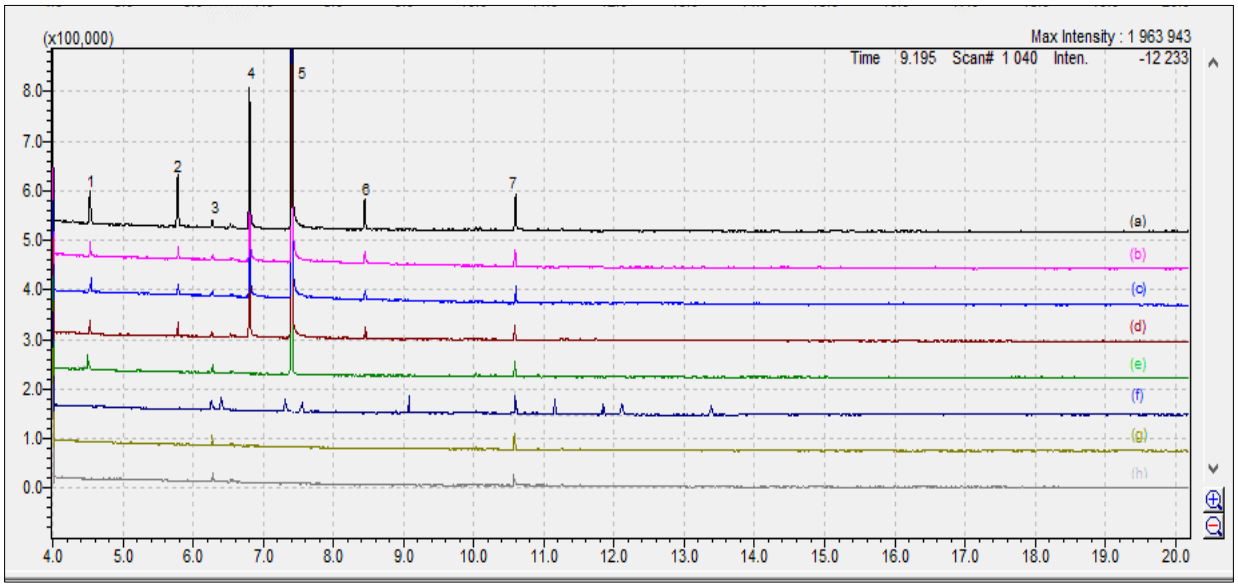

Fig.S-9. GC-MS chromatograms (a) Initial SPRW; (b) After 30 min heating; (c) After 30 min adsorption; (d) x:0.0; (e) x:0.5; (f) x:1.0; (g) x:1.5 and (h) x:2.0
(SPRW, H_2O_2/COD: 5, $Ni_{(2-x)}Cu_{(x)}$Al-LDH: 0.4 g L^{-1},
T: 60°C, reaction time: 90 min, pH: pH_{PZC})
1) Toluene; 2) Xylene; 3) Nonane; 4) Phenol; 5) O-Cresol; 6) Naphthalene; 7) Hexadecane

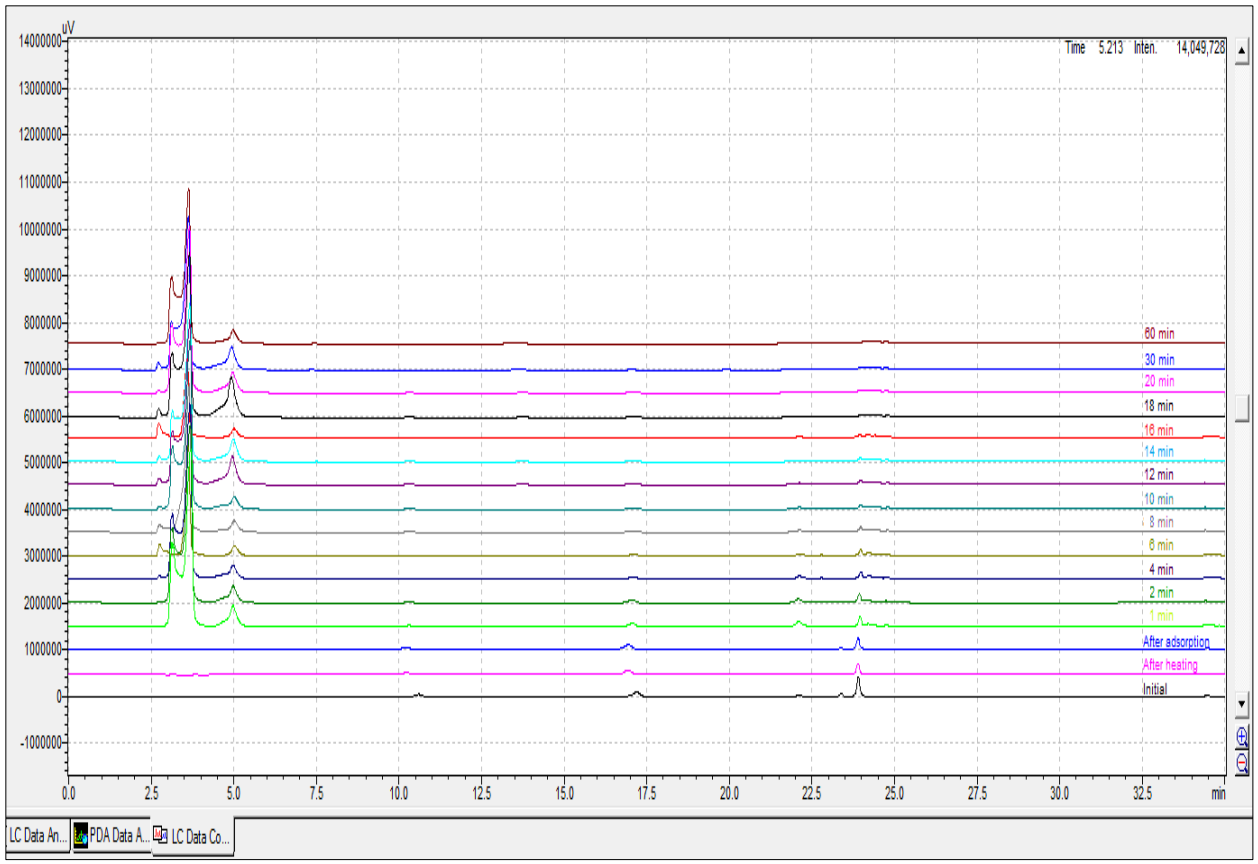

Fig.S-10. HPLC chromatograms of SPRW degradation at different reaction time (SPRW, H_2O_2/COD: 5, $Ni_{(2-x)}Cu_{(x)}Al$-LDH with x:1.0: 0.4 g L^{-1}, T: 60°C, reaction time: 90 min, pH: pH_{PZC})

6. Comparison of catalysis performance

Table S-4. Comparison of various copper-based LDH catalysts for the degradation of organic pollutants in wastewater.

Catalysts	*TOC removal (%) and/or Reduction efficiency (%)*	*Nature*	*Operating conditions*	*References*
CuNiAlCO_3-HTLc	47.1% Phenol conversion	Heterogenous Fenton reaction	Phenol: 0.5 g, Catalyst: 0.05 g, phenol/H_2O_2 (mol): 1/1.6, pH: 7, time: 1h, T:60°C.	(Zhu et al., 1998)
CuNiAl3-5 LDH	23.7% Phenol conversion	Heterogenous Fenton reaction	Phenol: 1.0 g/Water: 10 mL, catalyst: 10 mg, phenol/H_2O_2	(Dubey et al., 2002)

			(mol): 2.0, pH: 5.0, time: 2h, T:65°C.	
$CuNiAlCO_3$ LDH	80% TOC removal 100% Phenol conversion	Heterogenous Fenton reaction	Cu/Ni/Al: 4.8/1.2/ 2 molar ratio Phenol: 2.66 mM, Catalyst amount: 0.8 g L^{-1}, $n(H_2O_2)/n(Phenol)$: 15, pH: 6.5, time: 2h, T: 40°C.	(Zhou et al., 2011a)
CuNiAl35 LDH	62.8 ± 0.6% Phenol conversion	Heterogenous Fenton reaction	Phenol: 500 mg/Water: 10 mL, Catalyst amount: 17 mg, phenol/H_2O_2 molar ratio: 1:2, pH: 6.5, time: 2h, T:60°C.	(Dai et al., 2021)
CuNiAl35 LDH	60.5 ± 4.3% m-Cresol conversion	Heterogenous Fenton reaction	m-Cresol: 500 mg/Water: 5 mL, Catalyst amount: 17 mg, m-Cresol/H_2O_2 molar ratio: 1:2, pH: 6.5, time: 3h, T:60°C.	(Dai et al., 2021)
CuNiAl35 LDH	43.6 ± 3.5% 3-Ethylphenol conversion	Heterogenous Fenton reaction	3-ethylphenol: 500 mg/Water: 5 mL, Catalyst: 17 mg, 3-ethylphenol/H_2O_2 molar ratio: 1:2, pH: 6.5, time: 3h, T:60°C.	(Dai et al., 2021)
CuCo31 LDH	51.2% Phenol conversion	Heterogenous Fenton reaction	Phenol: 1.0 g/Water: 10 mL, catalyst: 10 mg, phenol/H_2O_2 (mol): 1/2, pH: 5, time: 2h, T:65°C.	(Rives et al., 2001)
CuMgAl-11 LDH	65.0% Phenol conversion	Heterogenous Fenton reaction	Phenol: 1.0 g/Water: 10 mL, catalyst: 10 mg, phenol/H_2O_2 (mol): 1/2, pH: 6.5, time: 2h, T:65°C.	(Kannan et al., 2005)

CuZnAl-LDH	100% Benzene conversion	Heterogenous Fenton reaction	Benzene: 5 g/Water: 15 mL, Catalyst: 10 mg, H_2O_2: 0.7 mL, time: 6h, T:50°C.	(Antonyraj & Kannan, 2011)
$Cu_{0.5}Ni_{2.5}Fe$ LDH	100% TOC removal	Heterogenous Fenton reaction	Phenol: 100 mg L^{-1}, Catalyst amount: 1.0 g L^{-1}, M_{H2O2}/M_{Phenol}: 56, pH: 6.5, time: 1h, T: 40°C.	(Hao Wang et al., 2018)
$Cu_1Ni_2Sn_{0.75}$ LDH	93.2% TOC removal	Heterogenous Fenton reaction	Phenol: 94 mg L^{-1}, Catalyst amount: 1.0 g L^{-1}, M_{H2O2}/M_{Phenol}: 56, pH: 6.9, time: 1h, T: 50°C.	(Hao Wang et al., 2020a)
$Ni_{(2-x)}Cu_{(x)}$Al-LDH x:1.0	65.24% TOC removal 100% Toluene conversion 100% Phenol conversion 100% o-Cresol 100% Xylene conversion 100% Naphthalene conversion	Heterogenous Fenton reaction	Mixture (Toluene, Nonane, Phenol, Xylene, Naphthalene, Hexadecane: 10 mg L^{-1}, o-Cresol: 20 mg L^{-1}), H_2O_2/DOC: 5, Catalyst: 0.4 g L^{-1}, pH : 7.5, time : 90 min, T: 60°C.	This work

Table S-5. Comparison of various copper-based non-precious metal catalysts for the degradation of organic pollutants in wastewater.

Catalysts	***TOC removal (%) and/or Reduction efficiency (%)***	***Nature***	***Operating conditions***	***References***
Cu/Ligand/H_2O_2 system	47.6% Benzene conversion 36.0% Toluene conversion	Homogenous Fenton reaction	Mixture (Benzene: 1.28 mM, Toluene: 1.09 mM, ethylbenzene: 0.94 mM, Xylenes:	(Baldrian et al., 2004)

	25.4% Ethylbenzene conversion 29.1% o-Xylene conversion 20.9% m-Xylene conversion 31.1% p-Xylene conversion		0.94 mM), $CuSO_4$: 10 mM, Succinic acid: 200 mM, H_2O_2: 100 mM, pH: 2-5, time: 20h, T: 22°C.	
Mesoporous $5Cu/Al_2O_3$–MCM-41 composite	70% 4-chloro-2-nitrophenol conversion 75% 2-chloro-4-nitrophenol conversión 80% Phenol conversion	Photo-Fenton reaction	Phenol, 2-chloro-4-nitrophenol, 4-chloro-2-nitrophenol: 100 mg L^{-1}/20 mL, Catalyst: 1 g L^{-1}, H_2O_2: 1.0 × 10^{-6} mol, pH: 4, time: 45 min, sunlight.	(Pradhan et al., 2013)
Copper loaded activated carbon	82% TOC removal 90% Nitrobenzene conversion	Heterogenous Fenton reaction	Nitrobenzene: 100 mg L^{-1}, Catalyst: 0.25 g L^{-1}; Cu loading: 2.5 wt%, H_2O_2/nitrobenzene (mol): 14.5, pH: 3, time: 4h.	(Priyanka et al., 2014)
Mesoporous carbon CuFe-MC-1-8 00 composite	83.7% TOC removal for phenol solution 66.3% TOC removal for bisphenol A solution 93.5% TOC removal for 2,4,6-Trichlorophenol	Heterogenous Fenton reaction	Phenol, Biphenol A, 2,4,6-Trichlorophenol: 100 mg L^{-1}, Catalyst: 300 mg L^{-1}, H_2O_2 : 30 mM, pH : 3, time : 12h, T : 25°C.	(Y. Wang et al., 2015)

Heterogeneous Fenton-like degradation of organic pollutants in petroleum refinery wastewater by copper-type layered double hydroxides

Ghania Radji,[1, 2 *] Nourredine Bettahar,[1] Abdellah Bahmani,[1] Ishak Boukhetache,[2] Sandra Contreras[3]

[1] *Laboratoire de chimie des matériaux inorganiques et applications (LCMIA). Université des Sciences et de la Technologie d'Oran Mohamed Boudiaf, USTO-MB, BP 1505, El M'naouer, 31000 Oran Algérie*
[2] *Faculté des sciences et de la technologie. Université Ahmed Draia, route nationale N°6, 01000 Adrar Algérie*
[3] *Departament d'Enginyeria Química, Universitat Rovira i Virgili, Av. Països Catalans 26, 43007, Tarragona, Spain*

Abstract

A series of $Ni_{(2-x)}Cu_{(x)}Al$-LDH layered ternary double hydroxides with x:0.0; 0.5; 1.5; and 2.0 were synthesized as catalysts to degrade aromatic and aliphatic organic compounds present in petroleum refinery wastewaters by means of a Fenton-type reaction and with hydrogen peroxide as a free radical generator. Samples obtained by coprecipitation at constant pH with a molar ratio $R:(Ni^{2+}+Cu^{2+})/Al^{3+}$ equal to 2.0 were characterized by PXRD, FT-IR, ESEM-EDS, ICP-OES, TGA and N_2 physisorption.

The results of the oxidation reaction showed that catalytic activity varied inversely with the Ni^{2+}/Cu^{2+} ratio, and activity was maximum for x:2.0. The catalyst can remove 74.8% of TOC, and the aromatic compounds can be completely oxidized by H_2O_2 after 90 min at 60°C under pH: pH_{PZC} conditions, a less excessive dosage of H_2O_2 (H_2O_2/COD:5), and a reaction medium temperature of 60°C. However, this catalysis presents phases other than LDH, such as malachite and gibbsite.

For lower Ni^{2+}/Cu^{2+} ratios, the highly dispersed MO_6 octahedra and the Jahn-Teller distortion effect facilitate electron transfer from Ni and thus increase the percentage of Cu^+, which can react with H_2O_2 to produce strong hydroxyl radicals. In the degradation process of aromatic organic compounds catalyzed by $Ni_{(2-x)}Cu_{(x)}Al$-LDH, hydrogen peroxide can first adsorb on the surface of the catalyst and then get an electron from Cu^+ ions to produce Cu^{2+}, $HO^{\bullet}$ and OH^- ions. $HO^{\bullet}$ can then react with the aromatic compounds to produce intermediates, organic acids, and alkanes. The presence of multivalent Cu, Ni and Al cations in LDH can build a closed electron cycle and rapidly regenerate Cu^+ species.

The catalytic oxidation process had first-order kinetics with an activation energy of 44.803 kJ mol^{-1} for the TOC disappearance reaction.

Keywords: Oil refinery wastewater; hydrotalcite-type; substitution effect; Fenton-like process; hydroxyl radicals.

* Corresponding author: Ghania RADJI
E-mail address: ghania.radji@univ-usto.dz
Phone: +213 772 880 292

1. Introduction

Given the considerable impact of industrial activities on the environment, pollution control is a major concern for the industrial sector. More restrictive environmental laws on waste or effluent disposal, industry pressure for environmentally sustainable practices, effluent disposal costs and, in some cases, water scarcity are all factors that have pushed for more stringent effluent treatment and reuse (Prado et al., 2020).

Petroleum refinery and petrochemical plants (PRPPs) are a collection of industries that are involved in the manufacture of fuels, lubricants and petrochemicals, as well as their intermediates and derivatives. As a result of global economic development and population growth, there is a significant increase in the demand for petrochemical goods (Jain et al., 2020). PRPPs consume a large amount of water in their various operations, such as cracking and distillation, and generate considerable volumes of wastewater (Hansen et al., 2018). PRPPs generate around 0.4 to 1.6 times the amount of crude oil produced (Coelho et al., 2006).

According to the IEA's reference scenario (which incorporates currently announced policies), by 2026 global oil consumption could increase to 104.1 mb/d, a 4% rise in the level prior to the Covid-19 pandemic (annual global oil demand are expected to exceed 2019 levels in 2023) (International Energy Agency, 2021). This consumption requires approximately 6,770 million liters of PRPP wastewater to be generated per day.

Scientists are concerned about the safety of the environment as a result of this surge in demand for PRPP goods. The reuse of water, then, in this area can give economic and environmental benefits.

The wastewater from petroleum refineries (PRW) contains a high concentration of aliphatic and aromatic hydrocarbons, which can cause significant contamination on the surface of soils and rivers (Sun et al., 2008). The United States Environmental Protection Agency (USEPA) has stated that phenolic derivatives are priority contaminants in water because of their extreme toxicity, stability, low biodegradability, and ability to persist in the environment for extended periods of time and harm the ecosystem. These hazardous contaminants are frequently present in industrial wastewater and can also cause a variety of operational problems: for example, corrosion of tubular equipment, scaling on the surface of heat exchangers, and environmental harm if the effluent is not properly treated before disposal. According to the United States Environmental Protection Agency (USEPA) and the World Health Organization (WHO), petroleum refinery wastewater (PRW) must be sufficiently treated to meet current regulatory requirements (Ghalehkhondabi et al., 2021).

PRW is extremely complex (Iqbal et al., 2017) and a variety of methods and technologies have been used to remove pollutants: , e.g., coagulation-flocculation and flotation (Santo et al., 2012) (Singh & Kumar, 2020), precipitation (Fu & Wang, 2011), adsorption (Dalanta et al., 2021) (Ulhaq et al., 2021), membrane filtration (Lebron et al., 2021), oxidation (Oller et al., 2011), bio-electrochemical oxidation and reduction

(Mohanakrishna et al., 2018), integrated treatment processes (Al-Mur et al., 2021), and bioremediation (Patel & Patel, 2020) (Ebrahimi et al., 2016).

All of these approaches, however, have significant drawbacks: due to the presence of hazardous aromatic and aliphatic hydrocarbons, as well as phenolic and refractory chemicals, biological processes alone are incapable of meeting reuse and discharge quality requirements (Vendramel et al., 2015) (Prado et al., 2020). Biodegradation takes longer to complete and is incompatible with most contaminants in the PRW (Molaei et al., 2022). Conventional methods such as adsorption, membrane filtration, and reverse osmosis transfer the pollutant from one medium to another, and the adsorbent's reusability is not guaranteed due to active site saturation (Ani et al., 2018).

In order to comply with increasingly stringent discharge criteria, effective advanced treatment procedures are required (Chen et al., 2017). Advanced oxidation processes (AOPs) produce radical entities, most notably hydroxyl radicals ($HO^{\bullet}$), which are the most powerful oxidizing species that can be used to treat water and industrial effluents (Domingues et al., 2022). $HO^{\bullet}$ is the second most reactive species after the fluorine atom; it attacks most organic pollutant molecules at a rate of 10^6–10^9 M^{-1} s^{-1}, which is 10^6–10^{12} times faster than ozone (Cheng et al., 2016), reacts with -C-C- double bonds and attacks aromatic rings, major components of refractory compounds (Gogate & Pandit, 2004). These processes can be used either as an oxidative pretreatment leading to readily biodegradable compounds or as a tertiary treatment for the elimination or complete mineralization of residual pollutants in CO_2, water, and inorganic salts (Gallard & Laat, 2000).

In this regard, the Fenton process, which decomposes hydrogen peroxide by redox reactions with iron (Eq.1) to generate hydroxyl radicals in solution (homogeneous processes) or at the interface with insoluble iron catalysts (heterogeneous processes), is considered to be one of the most effective advanced processes for treating oil refinery wastewater and reducing its pollutant content, odor and/or color (Tony et al., 2014):

$$Fe^{2+} + H_2O_2 \xrightarrow{k_1} Fe^{3+} + HO^{\bullet} + OH^- \qquad k_1 = 53 - 76\ M^{-1}\ s^{-1} \qquad \text{(Malato et al., 2009)} \qquad (1)$$

The principal Fenton oxidant ($HO^{\bullet}$) can be eliminated by an excess of iron (Eq.2) or hydrogen peroxide (Eq.3), which can reduce the efficiency of the homogeneous process. This means that the H_2O_2/Fe^{2+} ratio must be carefully chosen to prevent the oxidation effect (Domingues et al., 2018).

$$Fe^{3+} + H_2O_2 \xrightarrow{k_2} Fe^{2+} + HOO^{\bullet} + H^+ \qquad k_2 = 1 - 2 \times 10^{-2}\ M^{-1}\ s^{-1} \quad \text{(Malato et al., 2009)} \qquad (2)$$

$$HO^{\bullet} + H_2O_2 \xrightarrow{k_3} HOO^{\bullet} + H_2O \qquad k_3 = 3.3 \times 10^7\ M^{-1}\ s^{-1} \qquad \text{(Karthikeyan et al., 2012)} \qquad (3)$$

One of the advantages of this homogeneous process is that it does not require solid catalysts to be separated and reused. However, it does have several inherent drawbacks that restrict its widespread application. For instance, a strict pH range (acidic pH), high H_2O_2 consumption, and the accumulation of ferric sludge reduce the oxidation efficiency (N. Wang et al., 2015). Researchers have focused a great deal on enhancing the

Fenton process to overcome these drawbacks. Solid iron-based catalysts have been used to replace the homogeneous Fe^{2+} (Pourehie & Saien, 2020).

Once compared to iron-based catalysts, copper-based catalysts behave like Fenton-like catalysts even though hydroxyl radicals can be generated by the reaction, as shown by the following equation:

$$Cu^{+} + H_2O_2 \xrightarrow{k_4} Cu^{2+} + HO^{\bullet} + OH^{-} \qquad k_4 = 1.0 \times 10^4\ M^{-1}\ s^{-1} \qquad \text{(Qiao et al., 2012)} \qquad (4)$$

$$Cu^{2+} + H_2O_2 \xrightarrow{k_5} Cu^{+} + HOO^{\bullet} + H^{+} \qquad k_5 = 4.6 \times 10^2\ M^{-1}\ s^{-1} \qquad \text{(Qiao et al., 2012)} \qquad (5)$$

They exhibit higher leaching resistance, a better catalytic performance, and a wider range of pH operations than iron-based catalysts (Nichela et al., 2013).

In addition to reacting with the target substrates (S) (Eq.6), extremely reactive hydroxyl radicals may also react with the oxidant itself (Eq.3).

$$HO^{\bullet} + S \xrightarrow{k_6} Products \qquad (6)$$

In the last decade, there has been considerable interest in developing heterogeneous copper-based catalysts, particularly LDH compounds.

Layered double hydroxide compounds (LDH) are an interesting class of materials because of their anion exchange properties (Zhang et al., 2019) (Johnston et al., 2021), adsorption capacities (Kefif et al., 2019) (Bouteiba et al., 2020) (Bouteraa et al., 2020), catalytic and photocatalytic uses (Oladipo et al., 2019) (Oladipo, 2021) (Azalok et al., 2021) pharmaceutical applications (Nava-Andrade et al., 2021) (Bini et al., 2019), and usefulness in wastewater treatments (Rezak et al., 2021) (Guo et al., 2021).

Consisting of metal hydroxide layers with anions in the inter-layer space (see Fig.1), LDH are structurally similar to the mineral brucite [$Mg(OH)_2$] in which a fraction of M^{II} ions are replaced by M^{III} ions (Mallakpour & Khadem, 2017). They can be represented by the general formula: $[M^{II}_{1-x}M^{III}_{x}(OH)_2]^{x+}[A^{n-}]_{x/n}.zH_2O$, in which M^{II} and M^{III} cations disperse in an ordered and uniform manner in brucite-like layers, x is the $M^{III}/(M^{II}+M^{III})$ molar ratio ($0.20 \leq x \leq 0.40$), and A^{n-} is a compensation anion of charge (n-) that leads to the electro-neutrality of such LDH as Cl^-, NO_3^-, SO_4^{2-} and CO_3^{2-} (Liu et al., 2019) (Kameda et al., 2021), metal complexes (Behbahani et al., 2021), surfactants (Wu et al., 2021) or other ligands (Y. Yang et al., 2019).

Many divalent metals (Zn^{2+}, Ni^{2+}, Cu^{2+}, Co^{2+}, Fe^{2+}, Ca^{2+}, etc.) (Das & Parida, 2021) and trivalent metals (Cr^{3+}, Fe^{3+}, Co^{3+}, Mn^{3+}, V^{3+}, etc.) (X. Wang et al., 2017) can be combined to form LDH layers. One exception is Cu^{2+}, which in spite of a suitable ionic ray can form pure LDH accompanied by another divalent cation M^{II} such as Mg^{2+}, Co^{2+}, Zn^{2+}, Fe^{2+} or Ni^{2+} (Cavani et al., 1991). In this case, the ratio Cu^{2+}/M^{II} must be lower than or equal to 1.0. This Cu^{2+} behavior comes from the "*Jahn Teller*" effect: the ions d^9 electronic configuration leads to the formation of deformed octahedral sites (Hao Wang et al., 2018). As long as the Cu^{2+}/M^{II} ratio is lower than or equal to 1.0, the Cu^{2+} ions are inserted in the non-deformed octahedral position in the brucite-type layers. When the ratio is greater than 1.0, some of the Cu^{2+} ions may be located in nearby

octahedra, and the formation of copper hydroxides with distorted octahedra is energetically preferred to that of the LDH structure (Cavani et al., 1991).

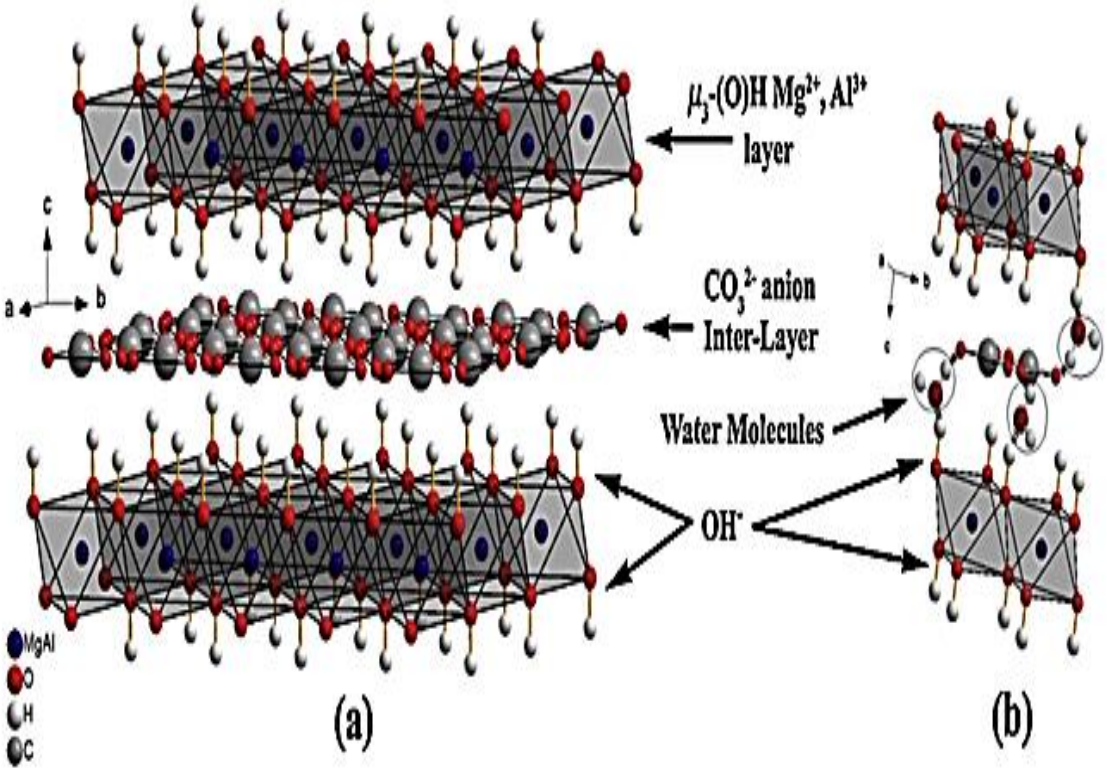

Fig. 1. (a) Schematic representation of the LDH structure; (b) Detailed schematic diagram of several physisorbed water molecules inside layers. Bonds illustrated as discontinuous squiggles attempt to convey the hydrogen bond interaction (Valente et al., 2012)

In a previous study (de Melo Costa-Serge et al., 2021), the catalytic activity of LDH containing magnesium, iron, and copper was evaluated in a heterogeneous Fenton process for the degradation of the antibiotic sulfathiazole. It was discovered that the addition of copper to the lamellar structure increased the material's specific surface area and degradation kinetics, allowing the antibiotic to be completely removed. This finding established the potential for copper-modified MgFe-CO_3 to be used as a catalyst to degrade developing pollutants, because it was straightforward to produce and extremely efficient in the Fenton process.

In other research, a series of ternary LDH based on CuNiFe (Hao Wang et al., 2018) and CuNiSn (Hao Wang et al., 2020) were synthesized as catalysts to degrade phenol via the Fenton reaction. The catalytic activity depends directly on the percentage of Cu^+, and activity is maximum at a Cu/Ni/Fe ratio of 0.5/2.5/1 and a Cu/Ni/Sn ratio of 1/2/0.75, which can mineralize 98.9% and 97% of phenol under mild conditions.

Building on previous work, this study aims to explore the effect of NiCuAl-LDH based catalysts on the Cu content when treating SPRW. It is hoped that these catalysts will improve the degradation of recalcitrant organic compounds and be viable alternatives to the conventional treatments used at present with these effluents.

2. Experimental

2.1. Preparation of catalysts

2.1.1. Materials

Nickel(II) chloride hexahydrate $NiCl_2.6H_2O$ (Sigma-Aldrich, 99.9%), copper(II) chloride dihydrate $CuCl_2.2H_2O$ (Sigma-Aldrich, 99.9%), aluminum(III) chloride hexahydrate $AlCl_3.6H_2O$ (Sigma-Aldrich, 99%), and sodium carbonate Na_2CO_3 (Biochem, 99.8%) were used to prepare the catalysts. Sodium hydroxide (Biochem, 97%) solution was used to adjust the pH.

2.1.2. Preparation of $Ni_{(2-x)}Cu_{(x)}Al$-LDH

To 200 mL of a solution of $NiCl_2.6H_2O$, $CuCl_2.2H_2O$ and $AlCl_3.6H_2O$, a mixture of a solution containing NaOH (1M) and Na_2CO_3 (1M) dissolved in distilled water was added dropwise at a constant rate (0.4 mL min^{-1}), under vigorous stirring for 3 h at room temperature. In all the cases studied, the molar ratio R between the bivalent and trivalent cations remained constant at 2.0 (M^{II} = 0.50 M and M^{III} = 0.25 M), and the nickel-substitution by copper changed from x:0.0 to x:2.0, although the nomenclature $Ni_{(2-x)}Cu_{(x)}$Al-LDH remained the same throughout. All syntheses were performed at pH 10.0 ± 0.2. To facilitate the crystallization of the precipitates, the contents were kept in a sealed vial at 70°C for 18 hours. The precipitates were then washed several times with distilled water to remove the chloride and sodium ions. Once the products had been purified, they were dried at 80°C for 20 hours and then ground to a homogeneous powder.

The synthesis protocol is represented by the flowchart in Fig.S-1 (Supplementary material).

2.2.Characterization techniques

The prepared catalysts were characterized by PXRD, FT-IR, TGA, ICP-OES, ESEM-EDS, and N_2 physisorption.

Powder X-Ray Diffraction (PXRD) measurements were performed using a Siemens D-500 diffractometer (Bragg-Brentano Parafocusing geometry and vertical - goniometer) equipped with a curved graphite diffracted-beam monochromator, incident and diffracted-beam Soller slits, a 0.06° receiving slit, and a scintillation counter as a detector. The range of angular 2 diffraction was between 5 and 70 degrees. The data were collected with an angular step of 0.05° and a sample rotation time of 3s per step. Cuk radiation was generated using a copper X-ray tube operating at a voltage of 40 kV and a current of 30 mA. The average crystallite sizes in the *c* direction (the stacking direction, perpendicular to the layers) of the LDH samples was estimated from the full width at half maximum (FWHM) values of the (0 0 3) and (0 0 6) diffraction peaks by means of the Scherrer equation and calculated using the X'pert HighScore Plus analysis software and the crystallinity index (CI) of the catalysts was measured by the PXRD technique. After subtracting the diffractogram of the amorphous phase from the whole diffractogram of the sample, the CI was calculated by

dividing the remaining area of the diffractogram of the crystalline phase by the total area of the original diffractogram (Park et al., 2010).

The infrared spectra (FT-IR) were acquired using KBr sampling on a Perkin-Elmer FT1730 spectrometer in the 4000-400 cm^{-1} range with 10 cm^{-1} resolution.

TGA was carried out using a SENSYS EVO TG-DSC (S60/58129, Setaram Instrumentation) in the presence of flowing Ar or synthetic air at a flow rate of 30 sccm. After a conditioning step of 300 seconds at 303 K, the crucible was heated to 1073 K at a rate of 10 K/min. After maintaining this temperature for 300 seconds, the chamber was allowed to cool for 1540 seconds. To determine the gas composition, the instrument outlet was connected to a mass spectrometer (MS, HiCube pumping station and PrismaPlus QMG220, Pfeiffer Vacuum).

ICP-OES analyses were carried out on aqueous samples of the catalysts following microwave digestion in a Milestone Ethos Easy digester. The analysis was performed using a 160 CCD spectrometer (Spectro Arcos).

ESEM analyses were conducted using a Quanta 600 Environmental Scanning Electron Microscope (FEI Company). EDS analyses were conducted with the aid of an Oxford Instruments EDS detector. The analyses were conducted in high vacuum mode with an accelerating voltage of 20 kV and a working distance of 10 mm. Micrographs were taken on gold-coated samples using a Q150R ES sputter coater (Quorum Technologies). The gold layer deposited was approximately 15 nm thick.

The BET surface areas, nitrogen adsorption-desorption, and pore size distributions of all catalysts were determined using the Brunauer-Emmet-Teller (BET) and Barrett-Joyner-Halenda (BJH) methods, respectively, via N_2 physisorption analysis using QuandraSorb SI Models 4.0 with the QuandraWin Software (quantachrome Instruments, v. 5.0 + newer) instrument at 77 K. Prior to measurement, each sample was outgassed at 373 K for 6 hours in the instrument pre-chamber (FloVac Degasser, Quantachrome Instruments) under vacuum (6 mTorr) to remove adsorbed species.

To determine the adsorption properties of our materials, the point of zero charge (pH_{PZC}) was determined using the salt addition method at room temperature as described by (Mak Yu et al., 2019): 1) an NaCl solution 0.01M was prepared; 2) 50 mL solutions were prepared with pH values between 2 and 12, which were adjusted by adding HCl (1M) or NaOH (1M); 3) 50 mg of each catalyst was placed in a solution and stirred for 24 hours; 4) after decantation, the final pH of the solution was measured and the curves drawn: $pH_f = f(pH_i)$ and $(pH_f\text{-}pH_i) = f(pH_i)$; pH_i and pH_f represent the initial and final pH of the solution, respectively.

2.3.Catalytic activity

2.3.1. Materials

The Fenton-like process was used to investigate the removal efficiency of aromatic and aliphatic hydrocarbons that are frequently detected in refinery wastewater. The composition of the synthetic petroleum wastewater (SPRW) was determined using data from prior research on real petroleum wastewater (RPRW)

(Aoudjit et al., 2018) (Demir-Duz et al., 2019) (Li et al., 2021).

Phenol (Sigma-Aldrich, 99-100%), naphthalene (Acros Orgnaic, 99%), toluene (Sigma-Aldrich, 99.5%), o-cresol (Sigma-Aldrich, 99%), xylenes (Panreac, 98%), nonane (Sigma-Aldrich, 99%) and hexadecane (Sigma-Aldrich, 99%) were used to prepare SPRW as the organic representatives of RPRW (Demir-Duz et al., 2019). Ammonium chloride, sodium chloride (Fulka, 99.5%) and sodium bicarbonate (Sigma-Aldrich, 99.9%) were used as inorganic representatives of RPRW (Demir-Duz et al., 2019). To emulsify nonane, hexadecane, and naphthalene, which are nearly insoluble in water, Triron^{TM} X-100 (Sigma-Aldrich) was used as a surfactant. Sodium hydroxide and sulfuric acid solution were used to adjust the pH. H_2O_2 (Acros Organic, 35 wt%) and sodium sulfite solution (Sigma-Aldrich, 40%) were used in Fenton-like experiments, dichloromethane (DCM, Sigma-Aldrich, 99.5%), acetonitrile (ACN, Reidel-de Haen, 99.9%) and phosphoric acid (Sigma-Aldrich, 85%) were used for analytical procedures.

2.3.2. Preparation of SPRW and water properties

To 5 mg of Triton X-100 and 900 mL of distilled water, the salts (ammonium chloride, sodium chloride and sodium bicarbonate) and insoluble components (nonane, hexadecane and naphthalene) were added in the required amounts (Table 1), and the solution was followed by the emulsification step with a homogenizer at 7000 rpm for 30 min. Then, the soluble organic components (phenol, toluene, cresol, and xylenes) were added to the required amounts of the mixture under continuous magnetic stirring at 450 rpm. Finally, the solution was made up to 1000 mL with distilled water and stirred for another 30 min. The salts were added before emulsification because they decrease the interfacial tension between the oil and the surfactant solution (Ferdous et al., 2012).

The composition and characterization of SPRW is given in Table 1.

Table 1. Composition and characterization of SPRW

Compounds	***Formulas***	***Concentration (mg L^{-1})***	***COD (mg L^{-1})***	***TOC (mg L^{-1})***
Toluene	C_6H_5-CH_3	10	31.26	9.12
Nonane	C_9H_{20}	10	34.95	8.42
Phenol	C_6H_6O	10	23.80	7.65
o-Cresol	C_7H_8O	20	50.31	15.54
Xylene	$C_6H_4(CH_3)_2$	10	31.65	9.04
Naphthalene	$C_{10}H_8$	10	29.96	9.36
Hexadecane	$C_{16}H_{34}$	10	34.62	8.48
Ammonium Chloride	NH_4Cl	70	-	-

Sodium chloride	NaCl	247	-	-
Sodium bicarbonate	$NaHCO_3$	160	-	-
TOTAL	**-**	**397**	**236.54**	**67.61**
pH		**8.0**		

247

248 *2.3.3. Treatment procedures*

249 Heterogenous Fenton-like process experiments were performed with 300 mL solution in a glass flask
250 equipped with a reflux condenser. Hydrogen peroxide (35 wt%) was added to the SPRW solution containing
251 the catalyst under magnetic stirring. The mixture was maintained at the desired reaction temperature. Fenton-
252 like experiments were performed for 90 min.

253 Various factors influencing the Fenton-like process were studied, such as the amount of catalyst, the
254 H_2O_2/COD ratio, the temperature of the reaction medium, and the solution pH. The H_2O_2/COD ratio (w/w)
255 was varied between 1 and 10, the catalyst concentration was varied between 0.1 and 1.0 g L^{-1}, and the
256 temperature of the reaction medium was adjusted between 30 and 70°C. Before the experiments, the pH of
257 the wastewater was adjusted to around pH_{PZC} in order to attain electrical neutrality on the catalyst surface,
258 except for the experiments in which the pH was varied between 5 and 9. The catalysts were added in the
259 required quantity. The reaction was then started by adding H_2O_2 while stirring continuously. At specified
260 intervals throughout the reaction, samples were taken to be examined and monitored using semi-quantitative
261 H_2O_2 strips to detect the remaining concentration of H_2O_2 in the samples. If H_2O_2 was detected in the samples,
262 sodium bisulfite was used to quench the reaction. According to analytical methods, samples collected during
263 the studies were centrifuged for 10 minutes at 5000 rpm.

264 All experiments were duplicated.

265 *2.3.4. Sample analysis*

266 Total organic carbon (TOC) measurements with a Shimadzu TOC-L analyzer were used to determine the
267 degree of mineralization during the studies. The following equation was used to determine the proportion of
268 TOC removed:

269 $$TOC\ removal\ (\%) = \frac{initial\ TOC - final\ TOC}{initial\ TOC} \times 100$$

270 Chemical oxygen demand (COD) was measured using the colorimetric method and the AQUALYTIC® Tube
271 Tests COD Vario.

272 The samples were analysed using HPLC in combination with a diode array detector (DAD) and GC-MS,
273 which provided qualitative and quantitative results. The extraction and analysis procedures are given in the
274 Supplementary material.

275

3. Results and discussion

3.1.$Ni_{(2-x)}Cu_{(x)}$Al-LDH catalyst characterization

3.1.1. PXRD

Assuming a *3R* layer assembly, the powder XRD patterns of the catalysts (Fig.2) are quite comparable to those commonly described in the literature for hydrotalcite materials intercalated with carbonate anions (PDF N°00-054-1030) (Barbosa et al., 2005) (Zhou et al., 2011a). The peaks at low angles, 2θ=11°, 23° and 35°, (d_{hkl}=7.60, 3.79 and 2.57Å, respectively) are attributed to the diffraction of the basal planes (0 0 3), (0 0 6) and (0 1 2). The base peaks get sharper and more intense as the copper concentration increases (from sample x:0.0 to sample x:2.0), suggesting that the solids become more crystalline as the copper content increases.

The (0 0 3) plane is typical of consecutive layer stacking along the *c* axis. Mesh parameter *c* is calculated by adding the thickness of the brucite layer (4.8 Å) and the thickness of the inter-lamellar space (about 2.82 Å for carbonate anions): i.e. the value of the inter-planar distance between the (0 0 3) planes. The latter is computed using the position of the first basal peak (0 0 3) in accordance with $c=3.d_{003.}$ The results are provided in Table 2.

The initial peak of the doublet, about 2=60°, is caused by the diffraction of plane (1 1 0), which is independent of the type of layers stacked and is used to determine cell parameter *a* (Cavani et al., 1991). The spacing between adjacent cations within a brucite-like layer is given by lattice parameter *a*, which is defined as $a=2.d_{110}$. A change in the cation results in an alteration of the *a* parameter (Å). Table 2 contains the values for the cell parameters of the samples.

Additionally, cell parameter *c* can be related to the columbic forces between the layers and the intercalated anion. There is no variation in the *c* values of the catalysts in this study, and the median value of d_{003} is 7.61 Å (C. Yang et al., 2016). The doublet size of nearly 2θ=60° increases from sample x:0.0 to x:2.0, and the two peaks are rather broad for sample x:0.0. Surprisingly, Ni^{2+} (0.72Å) has a higher ionic radius than Cu^{2+} (0.69Å). This phenomenon can be explained in part by the Jahn-Teller effect, which states that Cu^{2+} ions cause the formation of octahedral deformed hydroxyl groups, which involves an increase in the *a* parameter. The same phenomenon was observed when the ionic radius of the metal substituted in the $Mg_{1.95}M_{0.05}/Al_1$ (M: Ca, Sr, Ba) was increased (Valeikiene et al., 2020).

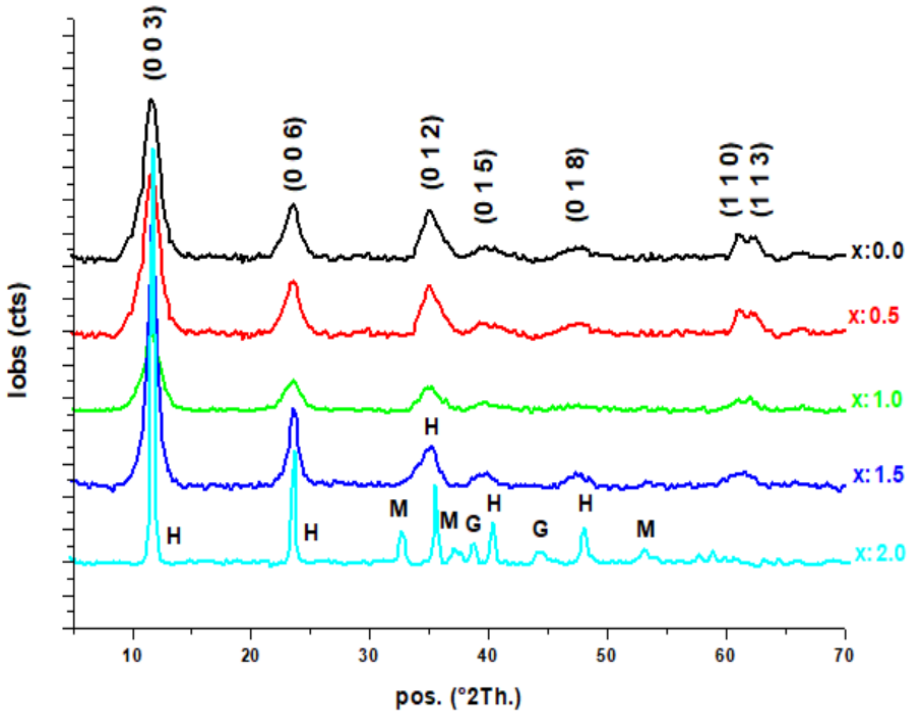

Fig.2. Powder X-Ray Diffraction (PXRD) patterns of $Ni_{(2-x)}Cu_{(x)}Al$-LDH with x:0.0; 0.5; 1.0; 1.5 and 2.0 catalysts

H: Hydrotalcite (00-054-1030), M: Malachite (00-001-0959) and G: Gibbsite (01-074-1775)

New lines appeared around 2θ=32°, 36°, and 53° that are characteristic of $Cu_2(OH)_2(CO_3)$-type malachite phases, and other lines appeared around 2θ=38° and 44° that are characteristic of $Al(OH)_3$-type gibbsite phases in samples x:1.5 and x:2.0. Consequently, a phase mixture exists for this material, which reduces its degree of purity. Britto (Britto & Vishnu Kamath, 2009) and Keffif (Kefif et al., 2019) came to the same conclusion.

A statistically significant increase in crystallite size (Table 3) was obtained with the increase in copper; and according to the X-ray diffraction analysis, the x:2.0 diffractogram shows better crystallization with a more intense characteristic peak (003), reflecting larger crystallite sizes with a crystallinity index of 99.36%, but with the presence of phases other than the LDH phase, such as malachite and gibbsite.

3.1.2. FT-IR

All of the bands observed in the FT-IR spectrum (Fig.3) were similar to those observed in a hydrotalcite-like phase with carbonate anions CO_3^{2-} as the inter-lamellar anion (C. Yang et al., 2016). Thus, the active absorption band in the range 3331-3400 cm^{-1} was attributed to the valence vibrations (stretching) of the -OH groups in the brucite layer and water molecules in the inter-lamellate space that are connected to carbonates via hydrogen bonds. The vOH band unfolds as a result of the appearance of a disordered structure. As the copper concentration increases, the band becomes sharper and shifts to higher wavenumbers, indicating that

the hydrogen bonding interaction between the laminae and the carbonate/water interlayer molecules increases.

A band at approximately 1640 cm^{-1} corresponds to the H-O-H bending vibration of water molecules in the inter-lamellate space (angular deformation) (Frost et al., 2003). This band shifts slightly to higher wavenumbers as the Cu content decreases.

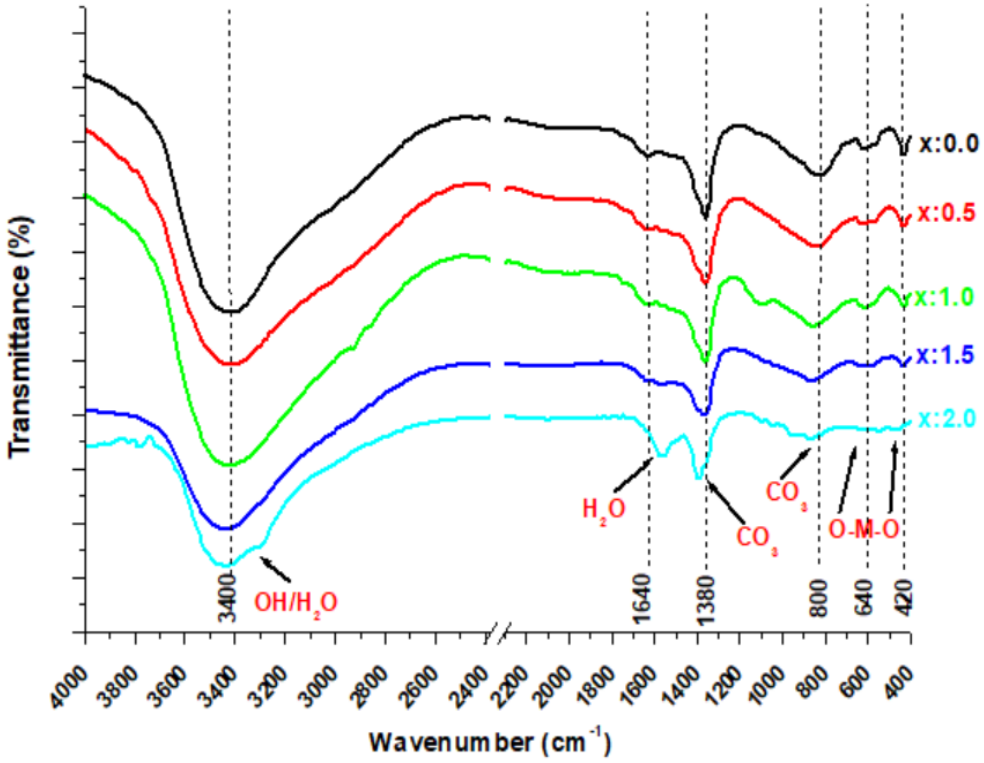

Fig.3. FT-IR spectra of $Ni_{(2-x)}Cu_{(x)}Al$-LDH with x:0.0; x:0.5; x:1.0; x:1.5 and 2.0 catalysts

The absorption band corresponding to the antisymmetric vibration mode of the carbonate anions in the interlamellar layers is located at 1369-1390 cm^{-1} (López et al., 1997). As the Cu content increases, this band shifts slightly to higher wavenumbers. The band was observed in all samples, indicating that the carbonate acts as a charge-balancing anion in the interlayer. Increased copper in the LDH phases decreases this band as the LDH phase decreases (results confirmed by PXRD). These band position changes are most likely caused by the Jahn-Teller distortion of the $Cu(OH)_6$ octahedra, which results in elongation along the *c*-axis (Å), facilitating hydrogen bonding with the interlamellar layer carbonate anion. Other carbonate anion vibrational modes (out-of-plane bending) appear between 880 and 800 cm^{-1}, and their intensity increases as the concentration of copper decreases, which is consistent with the PXRD results.

The bands below 600 cm^{-1} are attributed to the vibrational modes of the M-O (M: Al, Ni, Cu) metal-oxygen (Kloprogge & Frost, 1999) and M-OH metal-hydroxyl groups in the LDH lattice (Hui Wang et al., 2009), but a strict band assignment is difficult due to the complex band profile and band overlap when more than one metal is present (Palacio et al., 2010).

3.1.3. TGA

The thermogravimetric analysis (TGA), which shows how the mass of a sample varies with the temperature, is very useful for following the evolution of the composition. Generally, the thermal stability of LDH materials depends on such factors as the nature of cations, cationic compositions, the nature of inter-lamellar anions, the crystallinity of materials, etc. (Hui Wang et al., 2009).

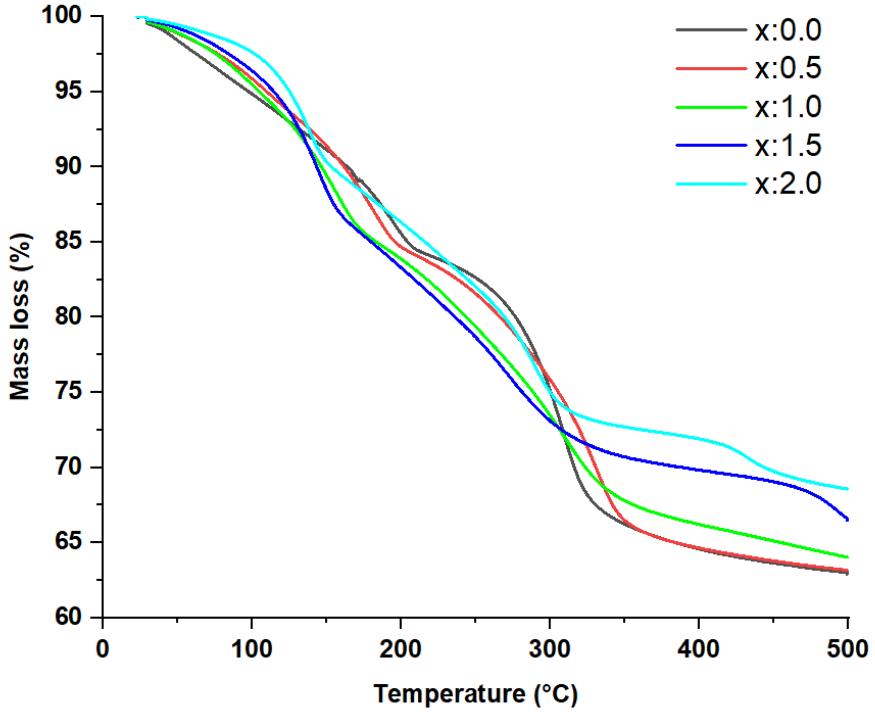

Fig. 4. TGA curves of $Ni_{(2-x)}Cu_{(x)}Al$-LDH with x:0.0; x:0.5; x:1.0; x:1.5 and 2.0 catalysts

The multi-step mass loss of type 4 according to the shape-based TG curve classification (Loganathan et al., 2017) was observed by examining the thermograms in Fig.4 of our $Ni_{(2-x)}Cu_{(x)}Al$-LDH catalysts with x:0.0; x:0.5; x:1.0; x:1.5 and 2.0. They revealed that our materials had undergone a multi-step decomposition process, as has often been reported in the literature (Cavani et al., 1991) (De Souza et al., 2012).

The hypotheses put forward to explain these losses, especially the most important ones, can be summarized as follows: 1) loss of physisorbed water between 60 and 200°C, 2) departure of structural water molecules between 200 and 350°C, 3) departure of a large portion of the carbonates, above 350°C, resulting in the destruction of the lamellar phase and the formation of oxides. Table S-1 (supplementary material) shows the total mass loss for each temperature range, as well as the total mass loss of our catalysts over a temperature range up to 500°C.

The results given in Table S-1 show a considerable decrease in mass loss between room temperature and 200°C when going from catalyst x:0.0 to catalyst x:2.0. This decrease was influenced by the mesh parameter, which increases from x:0.0 to x.2.0 (Table 3), and thus by the decrease in the charge density of the lamellae.

3.1.4. Elemental analysis

The characteristics of catalyst such as the chemical percentages of the elements in our samples, their empirical formulas, and the real molar ratios M^{2+}/Al^{3+} and Ni^{2+}/Cu^{2+} are recapped in Table 2.

Table 2. Elementary analysis of $Ni_{(2-x)}Cu_{(x)}Al$-LDH catalysts with x ranging from 0.0 to 2.0 by ICP-OES and TGA

Catalysts	*Compositions (mg L^{-1}) [a]*			*Total mass loss*	*Empirical formulas [b]*	*M^{2+}/Al^{3+}*	*Ni^{2+}/Cu^{2+}*
	Ni	*Cu*	*Al*	*(%)*		*(mol/mol)*	
x:0.0	39.102	-	08.069	37.00	$Ni_{0.666}Cu_{0.000}Al_{0.299}(OH)_2(CO_3)_{0.156}.0.1000H_2O$	2.22	∞
x:0.5	31.130	10.484	08.510	36.50	$Ni_{0.530}Cu_{0.165}Al_{0.315}(OH)_2(CO_3)_{0.156}.0.0656H_2O$	2.20	3.21
x:1.0	19.883	20.501	07.988	36.00	$Ni_{0.339}Cu_{0.323}Al_{0.296}(OH)_2(CO_3)_{0.155}.0.0633H_2O$	2.23	1.05
x:1.5	09.682	32.179	08.249	33.00	$Ni_{0.165}Cu_{0.506}Al_{0.306}(OH)_2(CO_3)_{0.156}.0.0583H_2O$	2.19	0.33
x:2.0	-	40.063	07.462	31.00	$Ni_{0.000}Cu_{0.630}Al_{0.276}(OH)_2(CO_3)_{0.152}.0.0385H_2O$	2.28	0.00

a Determined by ICP-OES
b Chemical formulas derived from ICP-OES and TGA results

The results obtained by ICP-OES in Table 2 show that the experimental molar ratio M^{2+}/Al^{3+} is very similar to the theoretical value of 2.0. In addition, and as far as the samples containing copper are concerned, the theoretical and calculated ratios are almost the same when Cu^{2+} substitution occurs. This means that the working conditions and the pH value chosen for the five multi-components synthesized were well respected. The following notation $Ni_{(2-x)}Cu_{(x)}Al$-LDH with x varying from 0.0 to 2.0 for sample identification was used in this study.

3.1.5. ESEM-EDS

Fig. 5 shows a spectrum of EDS analysis obtained from the catalyst powder with x:0.0; 1.0 and 2.0.

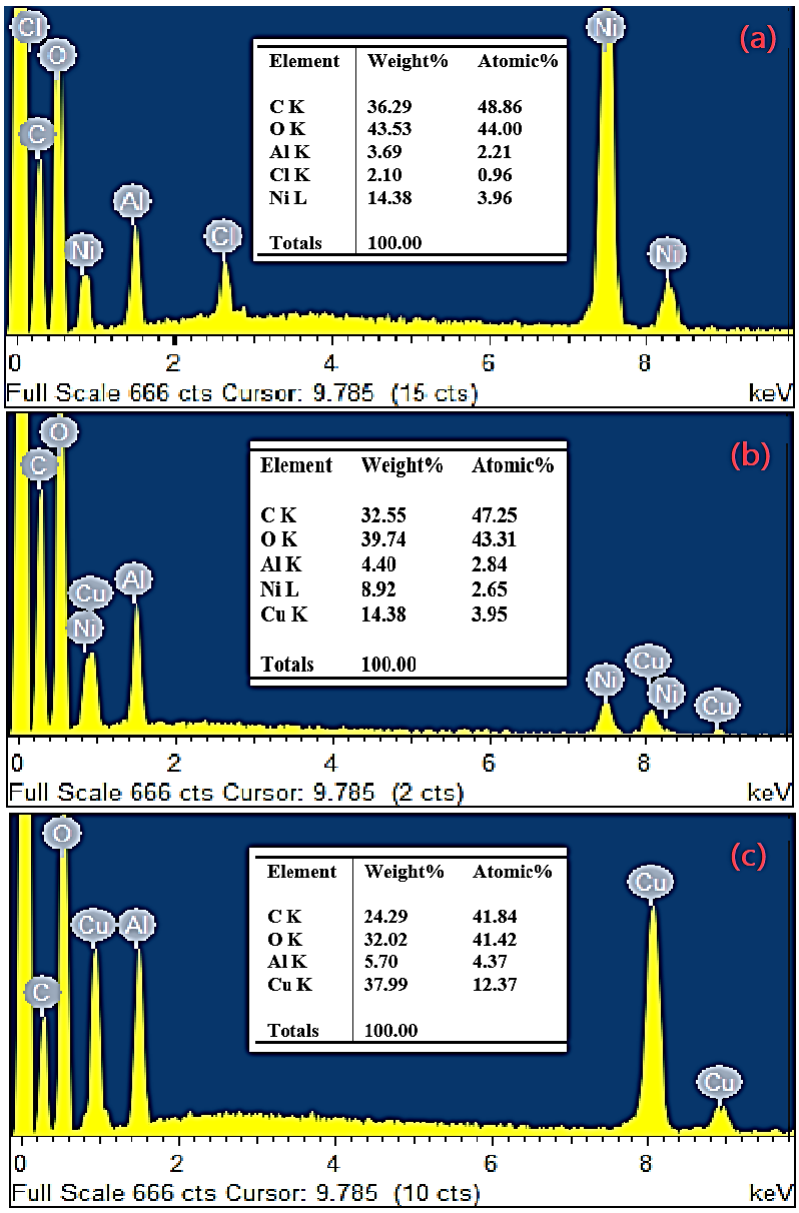

Fig.5. EDS analysis spectra of $Ni_{(2-x)}Cu_{(x)}$Al-LDH catalysts (a) x:0.0; (b) x:1.0 and (c) x:2.0

The EDS analysis of $Ni_{(2-x)}Cu_{(x)}$Al-LDH with catalysts x:0.0; 1.0, and 2.0 confirms that the material is composed of nickel, aluminum, copper, oxygen, and carbon (Figures 5-(a), (b), and (c)). These results attest to the formation of the hydrotalcite-type material and prove that the synthesized materials are pure, indicating that these materials are rigorously washed during synthesis, except for the material with x:0.0, which exhibits an unusual amount of chlorine.

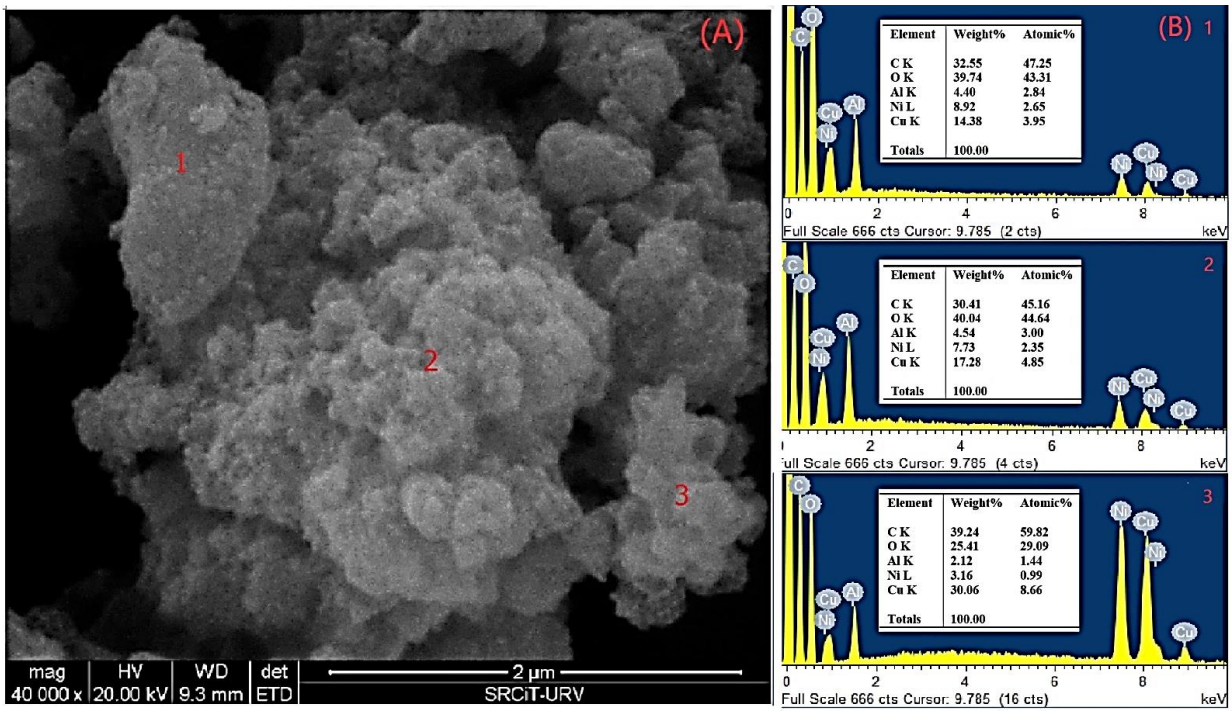

Fig.6. (A) Scanning electron microscopy (SEM) for $Ni_{(2-x)}Cu_{(x)}$Al-LDH catalyst with x:1.0 and (B) Energy-dispersion X-ray spectroscopy (EDS) in 1, 2 and 3 regions

The elements were semi-quantified by EDS analysis with the quantitative ZAF method (Dunn, 1989), and three points were measured in all samples. The content of Ni, Cu and Al is displayed in image 6-(B) confirming the substitution of nickel by copper in LDH.

As shown in Fig.7, the morphology of LDH was also influenced by the substitution of nickel with copper. Scanning electron microscopy images of $Ni_{(2-x)}Cu_{(x)}$Al-LDH for the x:0.0 catalyst shows the lowest level of crystallinity. This sample consists of a set of connected nanosheets, forming a sandy rose morphology, with the primary particle size being less than 20 nm and 100 nm in the smallest and largest dimensions, respectively.

The mechanism observed for the direct nanosheet growth with particles size reduction can be allotted to the increase in the nickel substitution by copper, while passing from the image (a) to the image (e). Indeed, the material for x:2.0 presents well crystallized particles of uniform size. By comparing these images obtained by SEM with the diffractograms of various nickel substitutions in Fig.3, the best crystallinity of the material x:2.0 can then be confirmed.

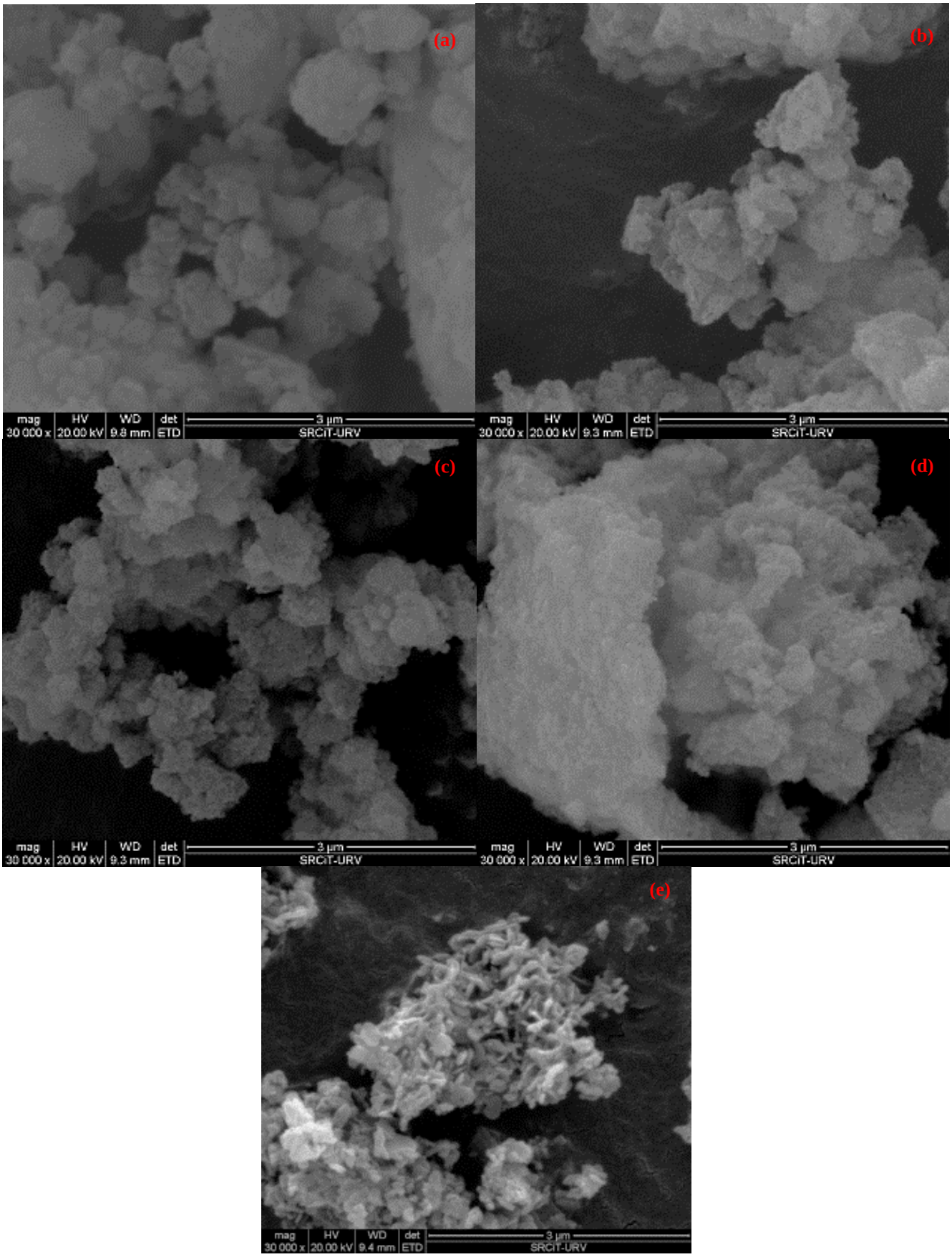

Fig.7. Scanning electron microscopy (ESEM) for $Ni_{(2-x)}Cu_{(x)}$Al-LDH catalysts (a) x:0.0; (b) x:0.5; (c) x:1.0; (d) x:1.5 and (c) x:2.0

3.1.6. N_2 physisorption

The N_2 adsorption–desorption isotherm and corresponding pore size distribution curve for the $Ni_{(2-x)}Cu_{(x)}Al$-LDH catalysts is shown in Fig.8.

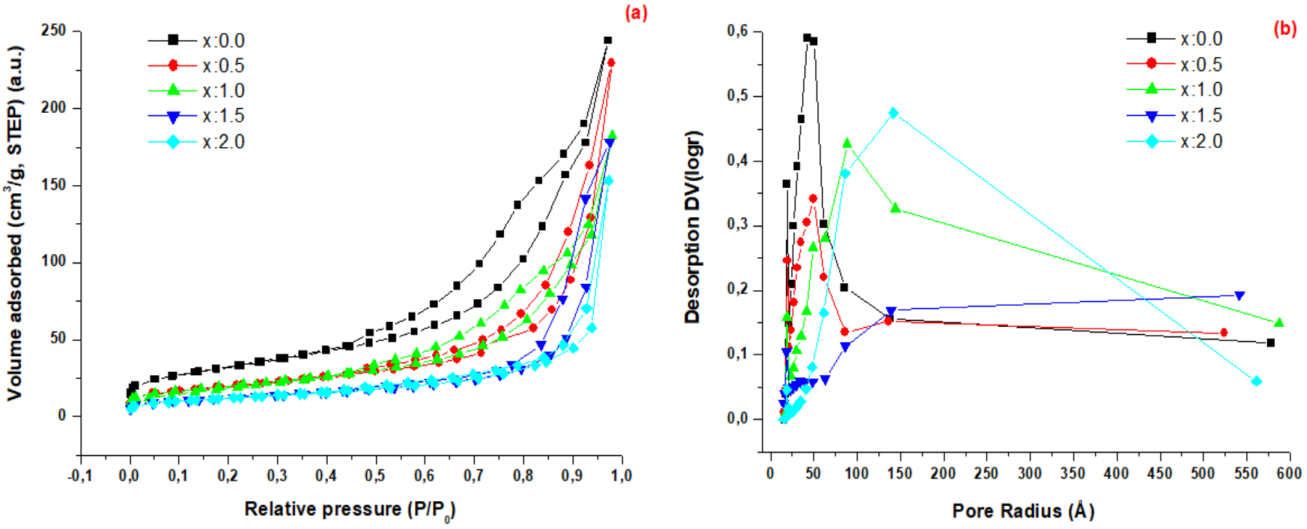

Fig. 8. (a) N_2 adsorption-desorption isotherms curves and (b) pore size distributions calculated from the branch of as-synthesized $Ni_{(2-x)}Cu_{(x)}Al$-LDH catalysts

All samples exhibit a characteristic *H3-type* hysteresis loop ($P/P_0 > 0.4$), typical of materials with slit-shaped pores formed by platelet aggregation, resulting in a broad pore size distribution (Fig.8-(b)) (Sing & Williams, 2004) (Bessaies et al., 2020). On the other hand, the N_2 adsorption/desorption isotherms revealed that the specific surface area gradually decreased from 147.5 to 40.8 m^2 g^{-1} and that the pore volume remained relatively constant at around 0.23–0.38 cm^3 g^{-1} as the Cu content increased. According to the IUPAC classification, all catalysts exhibited a type II isotherm, which is defined by the absence of a relative pressure plateau (P/P_0) near 1, indicating the presence of macropores. This *pseudo-type II* property is associated with the aggregate structure's non-rigidity.

For all catalysts, a sharp, high peak appears with a maximum around 3.7 nm. This shows that the small mesopores are responsible for the porosity characteristics of these materials. The PSD curve for the x:0.0 catalyst is wider and larger than the other catalysts. All pores are larger than 2 nm and no macropores larger than 50 nm were observed. Therefore, neither the micropores nor the uniformity of the pore structure is accentuated, except for the catalyst with x:2.0 which has a more uniform pore structure.

Table 3 shows the surface area, pore volume, and pore diameter.

3.1.7. pH_{pzc}

Fig. 9 depicts the pH_{PZC} curve for the $Ni_{(2-x)}Cu_{(x)}Al$-LDH catalysts. Three domains were found: 1) the domain in which $pH < pH_{PZC}$: pH_f increases with increasing pH_i; the surfaces of these LDH are positively charged due to the protonation process of the hydroxyl, so our sample becomes an anion adsorbent; 2) the domain in

which pH > pH_{PZC}: pH_f decreases with increasing pH_i; the surface of these LDH are negatively charged due to the deprotonation process of the hydroxyl, so our sample becomes a cation adsorbent; 3) the intermediate domain: pH_f remains constant with increasing pH_i and the point of zero charge pH_{PZC} is in this domain (Mak Yu et al., 2019). The pH_{PZC} values are represented in Table 3.

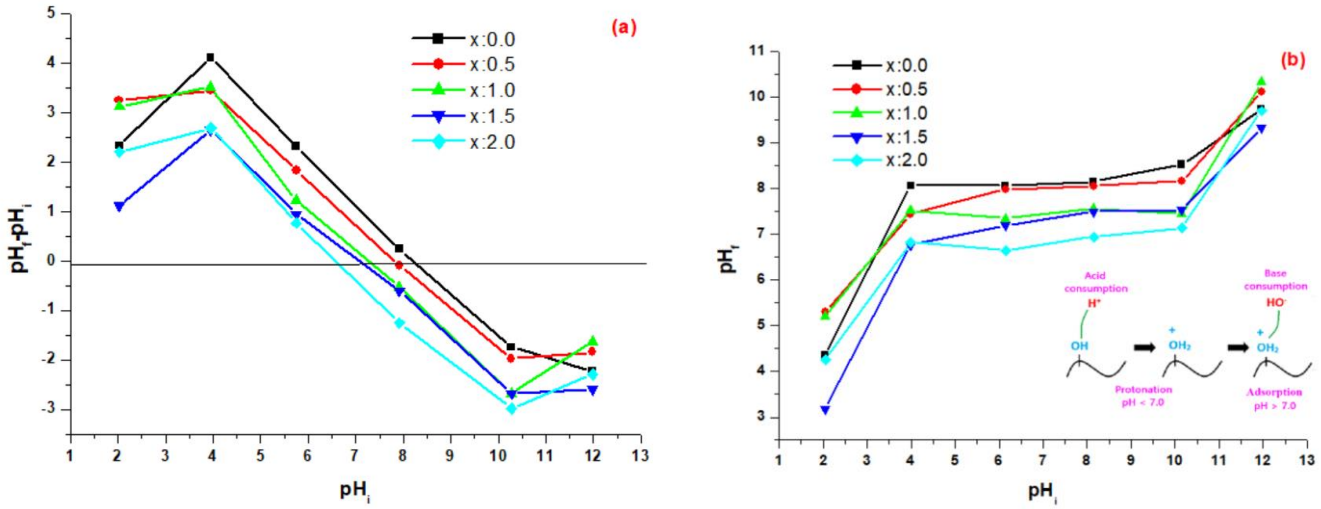

Fig.9. Plot of pH_{PZC} for the $Ni_{(2-x)}Cu_{(x)}Al$-LDH catalysts (a) pH_f-pH_i versus initial pH, (b) pH_f versus initial pH

Table 3. Lattice parameters, textural properties and pH_{PZC} of the catalysts

Catalysts	*Surface area S_{BET} ($m^2\ g^{-1}$)*	*Pore volume V_p ($cm^3\ g^{-1}$)*	*Average pore size d_p (nm)*	*pH_{PZC}*	*Crystallite size (nm) [a]*	*Crystallinity index (%) [b]*	*Lattice parameter*	
							c (Å) [c]	*a (Å) [d]*
x:0.0	147.5	0.388	3.818	8.10	06.60	90.40	22.92525	3.02474
x:0.5	96.6	0.359	3.816	8.00	09.65	92.90	22.86213	3.03504
x:1.0	81.5	0.293	3.799	7.50	12.80	94.71	22.84266	3.04428
x:1.5	49.5	0.278	3.788	7.20	26.60	94.78	22.78794	3.04914
x:2.0	40.8	0.234	3.729	6.90	115.80	99.36	22.72608	3.06544

[a] *Average crystallite sizes in the c direction using the Scherrer equation (calculated using X'Pert HighScore Plus software).*
[b] *Crystallinity index (%) calculated using OriginPro 2021 software.*
[c] $c = 3d_{0\,0\,3}$.
[d] $a = 2d_{1\,1\,0}$.

The relation between the pH_{PZC} value and the molar ratio (Ni^{2+}/Cu^{2+}) in the LDH phase is particularly noteworthy. A decrease in the molar ratio leads to a structural expansion and, therefore, to an increase in mesh parameter *a* and the inter-lamellar distance (results already confirmed by PXRD). In turn, there is a decrease in the charge density of the lamellae, and a decrease of the pH_{PZC} value, which has an influence on the adsorption yield.

3.2.Catalytic activity of the catalysts

3.2.1. Preliminary tests

Four preliminary tests of SPRW solution oxidation were carried out at 60°C:

- An initial SPRW oxidation reaction was carried out without a catalyst or H_2O_2;
- A second oxidation reaction was carried out in the absence of a catalyst and in the presence of hydrogen peroxide (H_2O_2);
- A third oxidation reaction was carried out in the absence of H_2O_2 and in the presence of a catalyst;
- A fourth oxidation reaction was carried out in the presence of hydrogen peroxide (H_2O_2) and the catalyst, .

Samples were analyzed by HPLC (Fig.S-2 and Fig.S-3) (Supplementary material). In the first three cases (without catalyst or oxidant, without catalyst, and without oxidant, Fig.S-2), the HPLC chromatograms obtained are identical to that of the initial solution, with the same retention times of the compounds, and with some reduction in TOC with values (16.04%, 16.09% and 20.03%, respectively). This reduction is due to the disappearance of 25.9%, 31.7% and 34.2% of toluene, respectively. Thus, for the third case, it should be noted that the process combines heating and adsorption on the surface of the catalyst. It should also be pointed out that the first reading of the HPLC chromatograms for the fourth case (Fig.S-3) shows that the compounds have almost totally disappeared and that 49.2% of TOC is removed after 60 min and 65.2% after 90 min of reaction. This proves that the oxidation reaction requires the presence of both the oxidant H_2O_2 and the catalyst.

GC-MS results (Fig.S-4) showed that all starting compounds remained stable in the first two tests (Fig.S-46(b) and (c)) (Supplementary material), no additional products appeared, phenols and naphthalene were totally oxidised after 90 min of treatment (Fig.S-4-(d)) and some alkanes (nonane and hexadecane) were still present.

According to the literature, aromatic organic compounds are degraded by LDH copper-based catalysts in the presence of hydrogen peroxide not because they are adsorbed by these catalysts but because a catalytically strong oxidant is produced, as has been demonstrated in several studies (Xie et al., 2021). It has been demonstrated that the hydroxyl radical can be formed during the degradation of hydrogen peroxide in the presence of transition metals (M) using the Fenton reaction (Eq.7) (Eroi et al., 2021):

$$M^{n+} + H_2O_2 \xrightarrow{k_7} M^{n+1} + HO^{\bullet} + OH^{-} \quad (7)$$

Copper-based layered double hydroxides have the ability to increase the reactivity of hydrogen peroxide by several orders of magnitude (Guo et al., 2020). In a heterogeneous medium, the pH of the medium has a significant impact on the process described above.

It is worth noting that these preliminary tests were carried out by fixing all the parameters: a H_2O_2/COD ratio equal to 5, the mass of the catalyst $Ni_{(2-x)}Cu_{(x)}$Al-LDH with x:1.0 equal to 1.0 g L^{-1}, the pH of the initial solution equal to pH_{PZC} and the temperature equal to 60°C.

Considering these aspects, we present the results on how the parameters influence the oxidation of SPRW in the presence of the x:1.0 catalyst. This catalyst was chosen for its pure structure and its copper-rich composition.

- influence of H_2O_2/COD ratio;
- influence of catalyst amount in solution;
- influence of reaction medium temperature;
- influence of initial pH solution.

3.2.2. Effect of parameters on SPRW degradation

The effect of H_2O_2 dosage and the amount of $Ni_{(2-x)}Cu_{(x)}$Al-LDH catalyst with x:1.0 on degradation were investigated. Fig.10-(a) and (b) illustrate the results obtained with a fixed catalyst concentration of 0.4 g L^{-1} and a variable H_2O_2/COD ratio, and a variable catalyst concentration and a fixed H_2O_2/COD ratio of 5, respectively. The importance of determining the optimal H_2O_2/COD ratio and amount of catalyst was clear, which is consistent with the findings of numerous studies on Fenton reactions.

The H_2O_2 dosage used in the Fenton reaction is a critical parameter in the process. All experiments were performed with pH adjustment: pH_{PZC}. No degradation is observed in the absence of H_2O_2, indicating that the adsorption of the compounds in these waters onto the catalyst is minimal.

In the Fenton-like experiments, the rates of TOC removed increased as the H_2O_2/COD ratio increased from 1 to 10; however, the increase in H_2O_2/COD was not evident at H_2O_2/COD ≥ 5 (Fig.10-(a)). A large excess of H_2O_2 may scavenge $HO^{\bullet}$ to produce less active $HO_2^{\bullet}$ radicals (Eq.3) (Xie et al., 2019). The $HO_2^{\bullet}$ produced can react with aromatic compounds; however, its oxidation capacity is lower than that of $HO^{\bullet}$.

$HO^{\bullet}_2$ consumes $HO^{\bullet}$ (Eq.8) when the concentration of $HO^{\bullet}_2$ is excessive in the system (X. Wang et al., 2021). Thus, TOC removal decreases. Considering the oxidation ratio of aromatic compounds and economy, the H_2O_2/COD ratio of 5 was reasonable under our experimental conditions.

$$HO_2^{\bullet} + HO^{\bullet} \xrightarrow{k_8} H_2O + O_2 \qquad k_8 = 0.71 \times 10^{10}\ M^{-1}\ s^{-1} \tag{8}$$

On the other hand, increasing the catalyst dosage from 0.1 g L^{-1} to 0.4 g L^{-1} significantly increased TOC removal at an H_2O_2/COD: 5 ratio. In contrast, when using a higher catalyst dosage (i.e., greater than 0.4 g L^{-1}), increasing the amount of catalyst used did not increase TOC removal (Fig.10-(b)). The same phenomenon was observed when phenol was catalytically oxidized with hydrogen peroxide on CuNiAl-CO_3 (Zhou et al., 2011b), which is probably explained by the fact that when the amount of catalyst was increased, the transfer resistance in the wastewater increased, hindering the contact between $HO^{\bullet}$ and organic pollutants from

SPRW. In addition, the decomposition rate of H_2O_2 increased, revealing the increase in the generation rate of $HO^{\bullet}$. However, these generated radicals cannot spread into the solution smoothly because of the mass transfer resistance. Instead, they react with each other and generate H_2O_2 again (N. Wang et al., 2021). To achieve a mineralization greater than 60% in 90 min, less than 0.4 g L^{-1} of catalyst and an H_2O_2/COD ratio of 5 was required.

Fig.10-(c) shows that TOC removal increases rapidly with temperature, reaching 7.2% and 65.9%, at 20°C and 70°C, respectively. Undoubtedly, higher temperatures (>70°C) would not be advisable considering the cost of the oxidation reaction and the accelerated decomposition of H_2O_2 at high temperatures according to equation (Eq.9).

$$2H_2O_2 \rightarrow O_2 + 2H_2O \quad (\Delta rH = -195{,}2\ \mathrm{kJ/mol}) \tag{9}$$

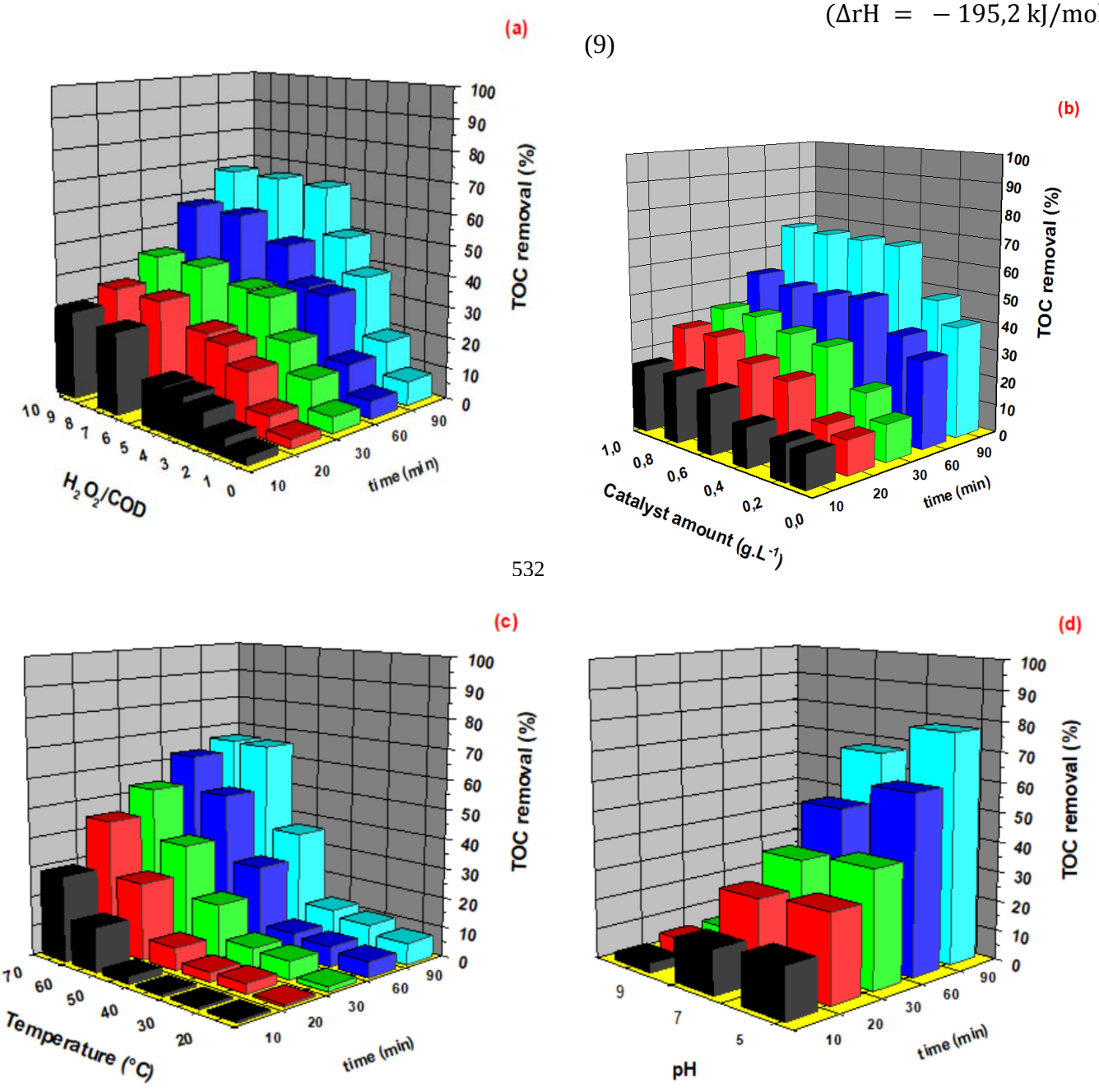

Fig.10. TOC removal rates depending on time and (a) catalyst amount, (b) H_2O_2/COD ratio, (c) temperature, (d) initial solution pH
(SPRW, H_2O_2/COD: 5, $Ni_{(2-x)}Cu_{(x)}Al$-LDH: 0.4 g L^{-1}, T: 60°C, reaction time: 90 min, pH: pH_{PZC})

The temperature at which SPRW is catalytically degraded by hydrogen peroxide is an important factor in the degradation process. Considering the main reactive oxidant $HO^{\bullet}$ in the Fenton-like process, the rate of disappearance of total organic carbon TOC is given by equation 10 (Qiao et al., 2012):

$$\frac{d[TOC]}{dt} = -k[TOC]^{\propto}[HO^{\bullet}]^{\beta} \quad (10)$$

where [$HO^{\bullet}$], [TOC], α, and β represent the concentrations of hydroxyl radicals, total organic carbon, the order of the reaction relative to the concentration of TOC, and the order of the reaction relative to the concentration of $HO^{\bullet}$, respectively.

The integral method and the differential method are the two fundamental strategies that we can use in the process of analyzing the data obtained from isothermal batch reactors.

This investigation focuses on the integral method (Werner J. A. Dahm et al., 1996), which begins with the functional form of a rate equation. The rate equation can be provided or a functional form proposed, such as first or second order. The rate equation is then inserted into the equilibrium equation and the equilibrium equation is integrated. The final step is to determine whether the integrated equation "fits the data" and, if so, the values of the rate coefficients. By "fit the data," we mean that the rate equation can predict how the experimental data change as the reaction time or initial concentrations vary.

For the equation proposed, let's first consider a first-order reaction for each reactant, where:

(1) The order of the reaction with respect to TOC concentration, α, is assumed to be equal to 1.

(2) The order of the reaction with respect to the concentration of $HO^{\bullet}$, β, is assumed to be equal to 1.

(3) The thermal energy source is held constant throughout the reaction,

Hypothesis (1) is widely accepted in both homogeneous and heterogeneous oxidation systems (Lam & Hu, 2013). Since the amount of catalyst and the volume of the reactor are constant, equation 10 can be rewritten as equation 11:

$$\frac{d[TOC]}{dt} = -k[TOC]^{1}[HO^{\bullet}]^{\beta} \quad (11)$$

There are three parts which influence the $HO^{\bullet}$ concentration: (1) the reaction between H_2O_2 and surface Cu species (Cu^{+}) leading to the formation of $HO^{\bullet}$ (as described in equation 12); (2) the reaction between SPRW and $HO^{\bullet}$ (as described in equation 13) and (3) the reaction between scavengers and $HO^{\bullet}$ (as described in Equations 14-16).

$$Cu^{+} + H_2O_2 \xrightarrow{k_{12}} Cu^{2+} + OH^{-} + HO^{\bullet} \qquad k_{12} = 1 \times 10^{4}\ M^{-1}\ s^{-1} \quad \text{(Gallard et al., 2019)} \quad (12)$$

$$TOC + HO^{\bullet} \xrightarrow{k_{13}} CO_2 + H_2O + \text{products} \qquad k_{13} = 10^{6} - 10^{9}\ M^{-1}\ s^{-1} \quad \text{(Haag \& David Yao, 1992)} \quad (13)$$

$$H_2O_2 + HO^{\bullet} \xrightarrow{k_{14}} HO_2^{\bullet} + H_2O \qquad k_{14} = 3.3 \times 10^7\ M^{-1}\ s^{-1} \quad \text{(Gallard et al., 2019)} \qquad (14)$$

$$HO_2^{\bullet} + HO^{\bullet} \xrightarrow{k_{15}} H_2O + O_2 \qquad k_{15} = 6.6 \times 10^9\ M^{-1}\ s^{-1} \quad \text{(Qiao et al., 2012)} \qquad (15)$$

$$HO^{\bullet} + HO^{\bullet} \xrightarrow{k_{16}} H_2O_2 \qquad k_{16} = 6 \times 10^9\ M^{-1}\ s^{-1} \quad \text{(Bokare \& Choi, 2014)} \qquad (16)$$

The decrease in $HO^{\bullet}$ was due to the last three reactions (14, 15 and 16), so the concentration of $HO^{\bullet}$ as a function of time can be described by equation 17:

$$\frac{d[HO^{\bullet}]}{dt} = k_{12}[Cu^+][H_2O_2] - k_{13}[TOC][HO^{\bullet}] - \sum_i k_i[S][HO^{\bullet}] \qquad (17)$$

where [S] represents the concentration of the scavengers in solution, and k_{12}, k_{13} and k_i represent the second-order reaction rate constants. Since these reactions reach steady state, the concentration of $HO^{\bullet}$ does not change with time, i.e.:

$$\frac{d[HO^{\bullet}]}{dt} = 0 \qquad (18)$$

Therefore, equation 20 can be obtained based on equations 17 and 18:

$$[HO^{\bullet}] = \frac{k_{12}[Cu^+][H_2O_2]}{k_{13}[TOC] + \sum_i k_i[S]} \qquad (19)$$

Adding equation 19 to equation 11, and assuming β=1, we obtain the following equation:

$$\frac{d[TOC]}{dt} = -k'[TOC]\frac{k_{12}[Cu^+][H_2O_2]}{k_{13}[TOC] + \sum_i k_i[S]} \qquad (20)$$

In this study, the H_2O_2 dosage is set at 1182.7 ppm to remove 67.61 ppm TOC. This value is eight times the stoichiometric ratio described in equation 21 for total mineralization containing 67.61 ppm TOC.

$$[TOC] \ll [H_2O_2] \qquad (21)$$

As mentioned above, a large number of $HO^{\bullet}$ radicals were consumed by multiple scavenger species in the reaction process. Therefore, it can be concluded that $k_{13}[TOC]$ is much smaller than $\sum_i k_i[S]$ and:

$$k_{13}[TOC] + \sum_i k_i[S] \approx \sum_i k_i[S] \qquad (22)$$

Here, Equation 20 can be simplified as:

$$\frac{d[TOC]}{dt} = -k_{app}[TOC] \qquad (23)$$

where k_{app} signifies the reaction's pseudo-first order rate constant in terms of TOC.

The solution of 23 is:

$$\ln\frac{[TOC]_t}{[TOC]_0} = -k_{app}.t \qquad (24)$$

The new constant k_{app} can be easily obtained from Eq.24 by plotting $\ln([TOC]_t/[TOC]_0)$ versus time, where k_{app} is the slope of the straight line.

Additionally, by applying the Arrhenius equation (N. Wang et al., 2021) (Eq.25) to the kinetic data at various temperatures, the activation energy of the oxidation process can be determined.

$$\ln k_{app} = \frac{-Ea}{RT} + \ln A \qquad (25)$$

where A is the frequency factor (min^{-1}), Ea is the activation energy (kJ mol^{-1}), R is the gas constant (8.314 J mol^{-1} K^{-1}), and T is the temperature (K).

By performing reactions at various temperatures (20, 30, 40, 50, 60, and 70 °C), the TOC disappearance concentration is measured as a function of reaction time, so that the corresponding values of $\ln([TOC]_t/[TOC]_0)$ can be determined (Fig.11). Lines represent the model fittings determined from equation 24 using the same reaction temperatures. A linear relationship with $R^2 > 0.94$ is obtained by comparing the experimental and fitted TOC concentrations, which shows that the assumption of $\alpha=1$ in Eq.10 is correct. The slopes of straight lines can be used to calculate the values of k_{app}, which are summarized in Table S-2 (Supplementary material). As the slope of the line ($\frac{-Ea}{R}$) in Fig.12 is equal to -5388.8, the activation energy (Ea) was calculated to be 44.803 kJ mol^{-1} during the disappearance of TOC.

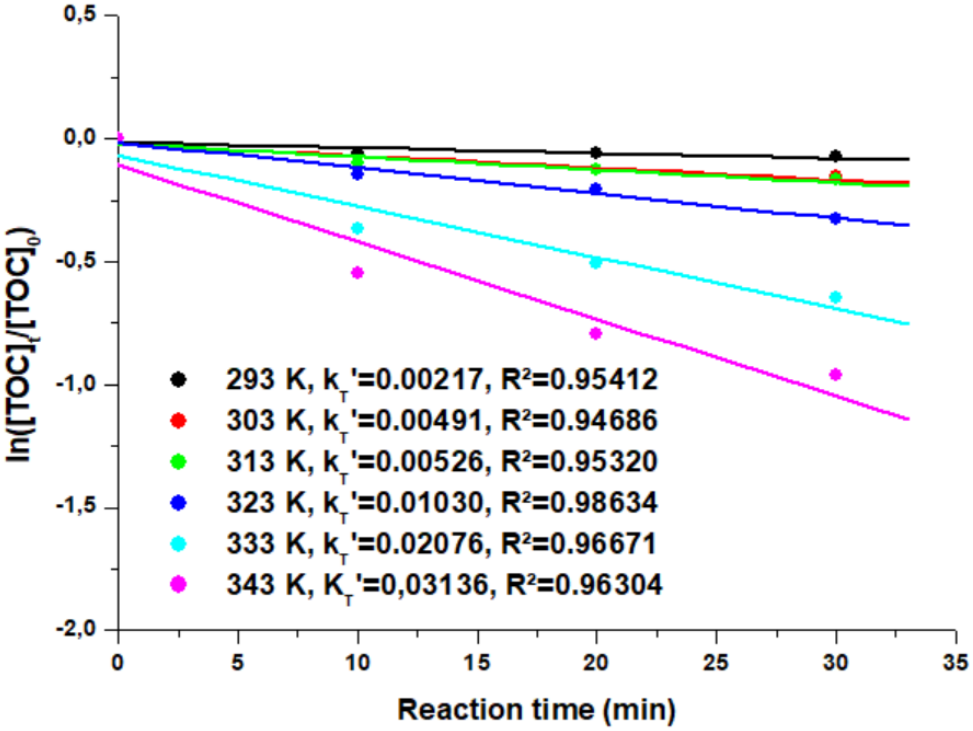

Fig.11. Disappearance rate of TOC in the SPRW degradation at different reaction temperatures using $Ni_{(2-x)}Cu_{(x)}$Al-LDH with x:1.0

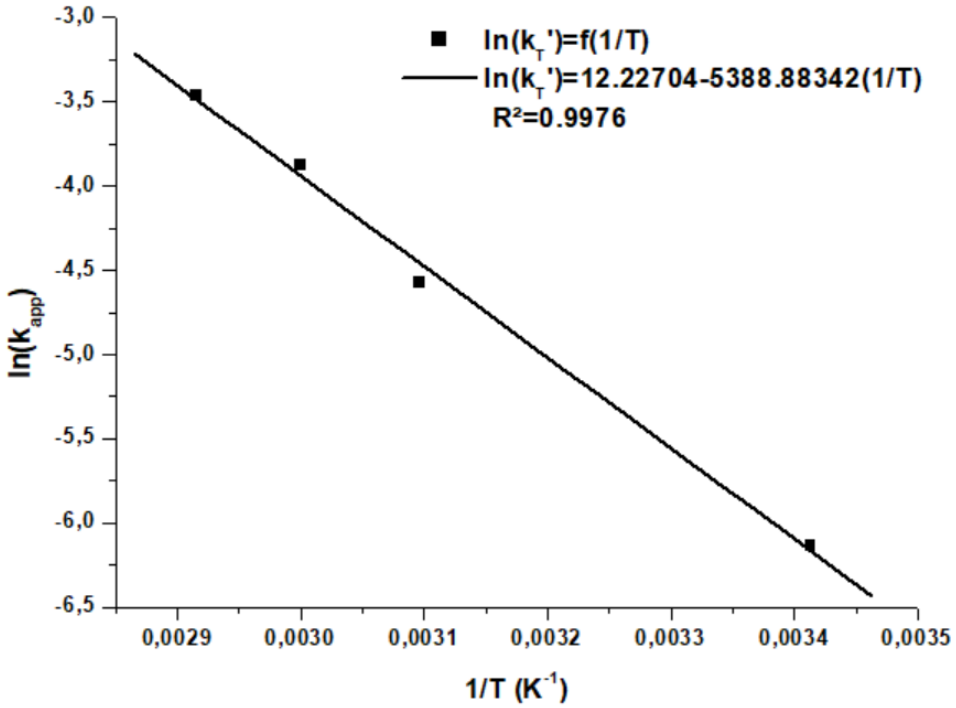

Fig.12. Effect of the temperature on the rate constant in TOC removal (SPRW, H_2O_2/COD: 5, $Ni_{(2-x)}Cu_{(x)}$Al-LDH with x:1.0: 0.4 g L^{-1}, reaction time: 90 min, pH: pH_{PZC})

The leaching of metals from the active species and the adsorption properties on the surface of catalysts were also influenced by the initial pH value; for these reasons, the initial pH plays an important role in the Fenton reaction and other reactions like it. Here, we studied the effect of pH on TOC removal from 0.4 g L^{-1} of $Ni_{(2-x)}Cu_{(x)}$Al-LDH with x:1.0 catalyst, in which the initial pH of the solution was adjusted with H_2SO_4 and NaOH. The results are shown in Fig.10-(d).

Adsorption tests lasting 30 minutes at pH 5, 7, and 9 on 0.4 g L^{-1} of $Ni_{(2-x)}Cu_{(x)}$Al-LDH with x:1.0 showed greater adsorption at acidic pHs than at basic pHs. The pH_{PZC} (zero charge point) of the x:1.0 catalyst is around pH 7.5. This catalyst's surface in water can be modeled as LDH≡Cu-OH, where it undergoes protonation or deprotonation depending on the pH of the solution. When the solution contains a great deal of H^+, protonation occurs on the catalyst surface (Eq.26), whereas when OH^- predominates, deprotonation occurs (Eq.27). On the surface of the catalyst, both protonation and deprotonation result in a positive and negative charge potential (Sá et al., 2013).

$$LDH \equiv Cu - OH + H^+ \rightarrow LDH \equiv Cu - OH_2^+ \quad (26)$$

$$LDH \equiv Cu - OH + OH^- \rightarrow LDH \equiv Cu - O^- + H_2O \quad (27)$$

The adsorption capacities were 7.60%, 4.64%, and 3.20% for pH 5, 7, and 9, respectively. This removal of TOC is mainly due to the adsorption of naphthalene (results confirmed by HPLC). The possible cation-π

interaction between the positive catalyst surface and the benzene ring of naphthalene may explain these results (Lam et al., 2021).

TOC removal was most efficient when the pH value was acidic (pH 5) (77.2% of TOC was removed after 90 minutes of oxidation reaction). This was due to the strong electrostatic attraction between the catalyst surface and hydrogen peroxide, which causes the latter to be rapidly adsorbed or gathered near the catalyst for activation. Since the charge density of the catalyst surface is not constant (i.e., it varies with pH), the force of attraction and the generation of radicals also vary. The rate of radical production increases proportionally with the charge density. However, a strongly acidic environment may be unfavorable for two reasons: first, it promotes metal leaching due to dissolution and thus the phase change (Yadav & Dasgupta, 2022) of the catalyst, which leads to the loss of active species and, since the heterogeneous reaction is the main driver of organic matter decomposition, a considerable decrease in the efficiency of the catalyst for reuse; second, hydrogen peroxide becomes more stable under strongly acidic conditions and forms oxonium and a large excess of H^+ ions (equations 28 and 29), which inhibit its reaction with the active species (Cu) to generate $HO^{\bullet}$ (Luo et al., 2020).

$$H_2O_2 + H^+ \rightarrow H_3O_2^+ \quad (28)$$

$$HO^{\bullet} + H^+ + \text{é} \rightarrow H_2O \quad (29)$$

At pH_{PZC}, the charge potential is neutral, and the surface charges on the catalyst equilibrate to a neutral state. In this state, hydrogen peroxide can only reach the catalyst surface through diffusion, which slows down the activation rate.

In alkaline solution (pH 9), after 90 min the removal of TOC decreased considerably (9.4%); this could be due to the generation of OH^- species, which prevent the adsorption of H_2O_2 and affect the generation of hydroxyl radicals once they approach the active center (Navalon et al., 2010). In addition, self-decomposition to H_2O and O_2 (Eq.9) in a strongly alkaline solution also reduces the efficiency of organic contaminant removal (Qiao et al., 2012). Related results show that H_2O_2 in alkaline solution can produce HO_2^- to consume $HO^{\bullet}$ and H_2O_2 by the following equations (30) and (31):

$$H_2O_2 \leftrightarrow HO_2^- + H^+ \quad (30)$$

$$HO^{\bullet} + HO_2^- \rightarrow H_2O + O_2^{\bullet -} \quad (31)$$

These results were confirmed by HPLC and GC-MS analyses, which showed the disappearance of aromatic components and the appearance of acids and other products at pH 5 and 7 (Fig.S-5 and Fig.S-6) (Supplementary material). These products are organic acids and alkanes almost all of which were nonanes and hexadecanes. At pH 9, it was noted that the starting chemicals remained unchanged, and no other by-products appeared.

The evolution of the pH during the experiments was also monitored, and the results indicate that it gradually declined as intermediates and/or organic acids were produced as oxidation products. This reduction in pH is significant because it can also impact the mechanism of the reaction.

Our catalysts were used with the pH adjusted to pH_{PZC} ($6.9 < pH_{PZC} < 8.1$), which is close to the pH of the solution (pH 8.0). This can simplify the pretreatment of wastewater, as the acidic pH is a pollutant factor, and also prevent equipment in the industrial sector from corroding and our materials from decomposing.

3.2.3. Effect of the substitution of nickel by copper on SPRW oxidation

In this section, the effect of substituting nickel by copper on the oxidation of organic compounds present in SPRW was examined by TOC analysis (Fig.13), HPLC chromatography (Fig.S-8) and GC-MS chromatography (Fig.S-9).

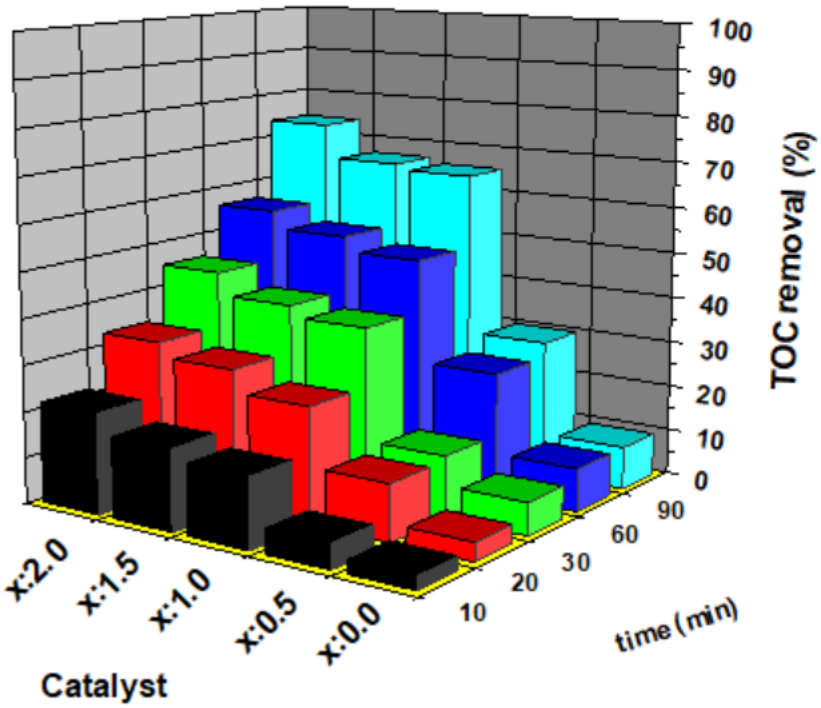

Fig.14. TOC removal rates depending on the time and effect of the substitution of nickel by copper on SPRW oxidation
(SPRW, H_2O_2/COD: 5, $Ni_{(2-x)}Cu_{(x)}$Al-LDH: 0.4 g L^{-1}, T: 60°C, reaction time: 90 min, pH: pH_{PZC})

$Ni_{(2-x)}Cu_{(x)}$Al-LDH with x to 0.0 from 2.0 were used as catalysts to degrade organic compounds present in SPRW via the Fenton-like reaction. The reaction conditions were chosen as the result of the previous series of experiments and have been mentioned above (pH: pH_{PZC}, H_2O_2/COD: 5, catalyst: 0.4 g L^{-1}, reaction temperature: 60°C and reaction time: 90 min).

Blank experiments were also performed at 60°C with (1) absence of both catalyst and hydrogen peroxide, (2)

absence of catalyst only and (3) absence of hydrogen peroxide only. TOC removal was about 14% for the first two experiments due to the thermal removal of a fraction of toluene and the persistence of all other starting products (results confirmed by HPLC and GC-MS), suggesting that the compounds contained in SPRW are difficult to mineralize in the absence of catalyst. For the third experiment the removal of TOC was 7.3%; 6.7%; 6.0%; 5.3% and 4.3% for catalysts with x:0.0; x:0.5; x:1.0; x:1.5 and x:2.0, respectively, due to a slight adsorption of naphthalene on the surface of the catalysts. The larger the surface area, the greater the removal (see Table 3). HPLC analysis shows that 51.4%, 47.8%, 42.8%, 40.9% and 25.5% of naphthalene was adsorbed on the surface of the catalysts with x:0.0, x:0.5, x:1.0, x:1.5 and x:2.0 after 30 min of adsorption at 60°C, respectively. It should be pointed out that the process is complex because it combines the thermal elimination of toluene and the adsorption of naphthalene. After 30 min, it is important to know if naphthalene was desorbed into the reaction medium or if it remained fixed on the surface of the catalyst. An infrared analysis (Fig.S-7) shows that new absorption bands appear: the first one between 3000 and 2800 cm^{-1} corresponds to the stretching =C-H bond; the second one between 1600 and 1430 cm^{-1} corresponds to the -C=C- stretching bond; the third one at 1100 cm^{-1} corresponds to the -C-H in plane bending bond; and the bands between 900 and 690 cm^{-1} correspond to the -C-H out of plane bending bond of the aromatic compounds. Comparing the spectrum of the catalyst after 30 min of adsorption with the spectrum of the same catalyst after 90 min of reaction, the same absorption bands were observed, showing the persistence of naphthalene on the catalyst surface.

Time 0 of the reaction started when hydrogen peroxide was added after 30 min of adsorption and the results of TOC removal are plotted in Fig.13. TOC removal increases with the decrease in the Ni^{2+}/Cu^{2+} ratio. For a Ni^{2+}/Cu^{2+} ratio of less than 1, more than 65% of TOC was removed.

In the coexisting system of catalyst and H_2O_2, the most active catalysts with x:1.0; 1.5 and 2.0 can mineralize not only the starting aromatic compounds but also the aromatic intermediates into molecular organic acids after 90 min of reaction.

Figures S-8 and S-9 (Supplementary material) illustrate the catalytic oxidation of organic compounds in SPRW using various catalysts. Activity was high for catalysts with x:1.0, x:1.5, and x:2.0. Additionally, given the low activity of x:0.0, it was clear that copper was the catalytically active phase (activation sites for hydrogen peroxide and organic molecules), as evidenced by the fact that TOC removal increased as the percentage of Cu^{2+} increased.

However, Fig.13 indicates that the introduction of nickel decreases TOC removal. It is important to mention that although TOC removal rates decrease to some extent with increasing nickel, the presence of nickel can weaken the Jahn-Teller distortion for copper-based LDHs (see Fig.2). Combining the characterization and activity results of $Ni_{(2-x)}Cu_{(x)}$Al-LDH, the structure-activity relationship of the compound can be derived.

As shown in Tables 3 and S-3 (Supplementary material), no correlation is observed between the activity and

the specific surface area of the catalysts. Therefore, the surface area of the $Ni_{(2-x)}Cu_{(x)}$Al-LDH catalysts seems to have little effect on catalytic activity: the catalysts with x:0.0 and x:0.5 have the highest specific surface areas 147.5 $m^2\ g^{-1}$ and 96.6 $m^2\ g^{-1}$, respectively, but are much less active than the catalysts with x:1.0, x:1.5 and x:2.0.

According to the results of HPLC analysis Fig.S-8 (Supplementary material), the aromatic organic compounds had completely degraded after 90 min of reaction for the catalysts with x:1.0, x:1.5 and x:2.0 and some acids and other by-products appeared at retention times between 2 and 7 minutes. These results were confirmed by the GC-MS analysis Fig.S-9 (Supplementary material). Nonane and hexadecane persisted for all the catalysts and phenol, toluene, o-cresol, xylene, and naphthalene completely disappeared for the catalysts with x:1.0, x:1.5 and x:2.0, while other alkanes and organic acids appeared. On the other hand, for catalyst x:0.0 no starting products disappeared, except for small fractions of toluene and naphthalene; and for the catalyst with x:0.5 traces of o-cresol and naphthalene were detected, always with the persistence of alkanes. At the given reaction time intervals, samples were taken and analyzed by HPLC. Taking into consideration the temperature of the reaction medium and its effect on the kinetics of the reaction, a quenching process was carried out; Fig.S-10 (Supplementary material) gives the HPLC chromatograms of the degradation of the aromatic organic compounds present in SPRW catalyzed by x:1.0. Although they cannot be identified separately, the main intermediates of the reaction were found to be aliphatic acids with retention times lower than 7 minutes (Naffrechoux et al., 2000).

During the first 30 min, the aromatic organic compounds decrease considerably at the same time as, the reaction intermediates form. These intermediates gradually decrease as the reaction time increases, and all the starting organic substances are completely degraded except the alkanes after 60 min.

Fig.13 shows that 6.3%, 28.7%, 65.2%, 66.9% and 74.8% of TOC was removed after a 90-min reaction catalyzed by the catalysts with x:0.0, x:0.5, x:1.0, x:1.5 and x:2.0, respectively. The remaining 34.7% 33.1% and 25.2% TOC for the catalysts with x:1.0, x:1.5 and x:2.0, respectively, consisted of starting nonane and hexadecane and the recalcitrant alkanes produced.

To be oxidized, these saturated molecules require very extreme reaction conditions or very strong reagents (Liu et al., 2019) because the lack of electron pairs in their components, carbon and hydrogen, means that they have recalcitrant properties (Rajasekhar Pullabhotla et al., 2008). Alkanes are oxidized by hydroxyl radicals when a hydrogen atom is abstracted to form water according to equation (32), while aromatic compounds are abstracted by electrophilic addition according to equation (33) (Zaviska et al., 2009).

1st case: elimination of a hydrogen atom

$$RH_2 + HO^{\bullet} \rightarrow RH^{\bullet} + H_2O \rightarrow hydroxylated\ products \quad (32)$$

2nd case: addition of the $HO^{\bullet}$ radical to the organic compound R

$$R + HO^{\bullet} \rightarrow RHO^{\bullet} \rightarrow oxidized\ products \quad (33)$$

3.2.4. *Proposed $Ni_{(2-x)}Cu_{(x)}Al$-LDH catalysis mechanisms*

The following is a mechanism based on electron transfer between metals in brucite-like sheets and the generation of $HO^{\bullet}$ radicals:

Since H_2O_2 is considered to have a skewed chain structure, the binding energies between two atoms in hydrogen peroxide are useful for estimating the formation of active species in degradation (Zhu et al., 1998). The O-O bond is easier to break than the O-H bond, and the p-orbitals along the direction of the O-O bond in the H_2O_2 molecule can obtain an electron from another substance such as Cu^{+} to produce $HO^{\bullet}$ and OH^{-}, according to equation (4).

In the degradation process of aromatic organic compounds catalyzed by $Ni_{(2-x)}Cu_{(x)}$Al-LDH, hydrogen peroxide can first adsorb on the surface of the catalyst and then get an electron from Cu^{+} ions to produce Cu^{2+}, $HO^{\bullet}$ and OH^{-} ions. $HO^{\bullet}$ can then react with the aromatic compounds to produce intermediates, organic acids, and alkanes. Finally, Cu^{2+} can be easily reduced by electron transfer between Ni^{2+} and Cu^{2+} in the brucite-like sheets, according to reaction (34), and the highly dispersed MO_6 octahedra in LDH also facilitate electron transfer (Mohapatra Lagnamayee, 2014). The quencher test should be performed for proving the $HO^{\bullet}$ radicals formation (J. Yang et al., 2022).

$$Cu^{2+} + Ni^{2+} \rightarrow Cu^{1+} + Ni^{3+} \quad (34)$$

However, the influence of the trivalent metal in LDH on the catalytic activity requires further study.

In addition, the abundance of hydroxyl groups on the surface of the LDH sheets can have positive effects on catalytic activity: they make LDH very hydrophilic, promote the proximity of organic compounds and hydrogen peroxide to active sites and the well-ordered layer structure can provide a lot of space, which is important for the degradation reaction (Rives et al., 2003). This result was confirmed by calcining the catalyst with x:1.0 at 320°C to obtain mixed metal oxides. Based on TGA analysis, this calcination decomposes these hydroxyl groups, and destroys the lamellar structure of LDH. A loss of catalytic activity was observed in the calcined material, in which TOC removal is reduced from 65.2% to 47.8%. It should also be pointed out that the presence of anions in solution can also play a role in the degradation performance, because this presence of anions in solution makes the structure of calcined LDH well-ordered because of the memory effect of LDH (Gao et al., 2018).

In summary, based on the above discussion, the $Ni_{(2-x)}Cu_{(x)}$Al-LDH catalyst with x:1.0 is probably the best of the catalysts tested: it has not only Cu^{+} cations as the catalytic active species, but also a well-ordered and well-crystallized pure LDH structure.

3.2.5. *Stability of catalyst during regeneration*

A comparison of catalytic performance in multiple tests had been performed to check the stability of $Ni_{(2-x)}Cu_{(x)}$Al-LDH catalyst with x:1.0. This catalyst was recovered by simple filtration, washed, and dried. Then

it was reused for SPRW degradation. HPLC results showed that this catalyst could still mineralize 100% of aromatic organic compounds after five runs. After the fifth reuse, the conversion rate decreased with the number of reuse cycles. This decrease is probably due to the adsorption of naphthalene on the catalyst surface, which prevents the contact between hydrogen peroxide and the catalyst surface from producing the hydroxyl radicals.

3.2.6. Comparison of catalysis performance

The efficiency of the $Ni_{(2-x)}Cu_{(x)}Al$-LDH catalyst prepared was compared with ternary copper-based catalysts for the degradation of organic pollutants in wastewater and the results are presented in Table S-4 (Supplementary material). Previous studies (Zhu et al., 1998) (Dubey et al., 2002) (Zhou et al., 2011a) (Rives et al., 2001) (Kannan et al., 2005) (Hao Wang et al., 2018) (Hao Wang et al., 2020) have reported that copper-based catalysts can catalyze the Fenton-like reaction of phenol. However, in the literature, few studies apply AOP to treat petroleum refinery wastewater, and most of the ones that do use synthetic or real single component wastewater (Antonyraj & Kannan, 2011) (Dai et al., 2021). In addition, they usually use such high amounts of reagents that they are above the discharge limits (Coelho et al., 2006) (Santos et al., 2006) (El-naas et al., 2014).

This study confirmed that the $Ni_{(2-x)}Cu_{(x)}Al$-LDH with x:1.0 catalyst can catalyze the Fenton-like oxidation reaction not only for phenol but also for a mixture of aromatic organic compounds such as phenol, toluene, o-cresol, xylene, and naphthalene, using water as the reaction medium. The parameters influencing the oxidation reaction were optimized, and the results confirmed that only 0.4 g L^{-1} was required to reduce TOC. However, other copper and non-precious metal catalysts (Baldrian et al., 2004) (Pradhan et al., 2013) (Priyanka et al., 2014) (Y. Wang et al., 2015) for the degradation of organic pollutants in wastewater have been studied in the literature (Table S-5, Supplementary Material). It should be noted that in many cases, acidic solutions or toxic organic solvents have been used to effectively regenerate copper-containing catalysts, while simple sample filtration has been successfully applied for the regeneration of the $Ni_{(2-x)}Cu_{(x)}Al$-LDH catalyst.

4. Conclusions

SPRW was treated efficiently by a $Ni_{(2-x)}Cu_{(x)}Al$-LDH catalyzed Fenton-like process with x:0.0, x:0.5, x:1.0, x:1.5 and x:2.0. The preparation and characterization of the catalysts, optimization of the SPRW treatment process, degradation kinetics of organic compounds, and pre-improvement mechanisms of $Ni_{(2-x)}Cu_{(x)}Al$-LDH catalysis were studied. The conclusions are as follows:

(1) The $Ni_{(2-x)}Cu_{(x)}Al$-LDH catalyst with x:1.0 seems to be the best of the prepared catalysts, in terms of crystallinity and purity.

(2) The substitution process of nickel by copper in the LDH phase varied the structure, porosity, and

morphology of the catalysts:

- The interlamellar space decreased and the distance between the two adjacent atoms increased, which is surprising because the ionic radius of nickel is larger than that of copper. For copper-rich catalysts (x:1.5 and x:2.0), new phases such as malachite and gibbsite appeared with the hydrotalcite-type phase.
- The decrease in the mass loss between room temperature and 200°C corresponds to the loss of the physisorbed water molecules at the surface of the catalyst and was influenced by the mesh parameter *a* and thus by the decrease in the lamellar charge density.
- A type II adsorption isotherm was observed forming interparticle porosity, with a progressive decrease in specific surface area and a large H3 type hysteresis loop with slit-shaped pores formed by platelet aggregation.

(3) Blank experiments for SPRW treatment at 60°C showed thermal removal of a toluene fraction and slight adsorption of naphthalene on the catalyst surface.

(4) Under the optimal SPRW treatment conditions (H_2O_2/COD: 5, catalyst amount: 0.4 g L^{-1}, pH: pH_{PZC}, reaction time: 90 min and temperature: 60°C), the catalytic activity of the $Ni_{(2-x)}Cu_{(x)}$Al-LDH catalyst increases with increasing copper content. The catalyst with x:2.0 shows the highest activity, a TOC removal of 74.8%. It should be noted that this catalyst presents phases other than the hydrotalcite phase such as malachite and gibbsite.

(5) $HO^{\bullet}$ radicals might play a leading role in the degradation of aromatic organic compounds present in SPRW and the rate at which they are generated can be accelerated by increasing the Cu^{+} content on the catalyst surface.

(6) TOC abatement follows the pseudo-first order kinetic model with an activation energy value of Ea: 44.80 kJ mol^{-1}.

This is only an initial study, and further studies on the potential application of the catalysts in actual wastewater treatment will be needed in order to alleviate production pressure.

Acknowledgement

Ghania RADJI gratefully acknowledges the Algerian Ministry of Higher Education and Scientific Research for funding her internship at the Universitat Rovira i Virgili in Tarragona (Spain) under the exceptional national program PNE 2019-2020. She also acknowledges the General Directorate of Scientific Research and Technological Development (DGRDT) (Algeria), the Technical Platform of Physicochemical Analysis (PTAPC-Laghouat-CRAPC) (Algeria), and all members of the three laboratories.

Appendix A. Additional data

Supplementary material for this article is available online at doi:

References

Al-Mur, B. A., Pugazhendi, A., & Jamal, M. T. (2021). Application of integrated extremophilic (halo-alkalo-thermophilic) bacterial consortium in the degradation of petroleum hydrocarbons and treatment of petroleum refinery wastewater under extreme condition. *Journal of Hazardous Materials*, *413*(January), 125351. https://doi.org/10.1016/j.jhazmat.2021.125351

Ali, B., Naceur, B., Abdelkader, E., Karima, E., & Nourredine, B. (2020). Competitive adsorption of binary dye from aqueous solutions using calcined layered double hydroxides. *International Journal of Environmental Analytical Chemistry*, *00*(00), 1–20. https://doi.org/10.1080/03067319.2020.1766035

Ani, I. J., Akpan, U. G., Olutoye, M. A., & Hameed, B. H. (2018). Photocatalytic degradation of pollutants in petroleum refinery wastewater by TiO2- and ZnO-based photocatalysts: Recent development. *Journal of Cleaner Production*, *205*, 930–954. https://doi.org/10.1016/j.jclepro.2018.08.189

Antonyraj, C. A., & Kannan, S. (2011). Influence of co-bivalent ions in cu-containing ldhs and solvent on hydroxylation of benzene to phenol. *Applied Clay Science*, *53*(2), 297–304. https://doi.org/10.1016/j.clay.2011.01.024

Aoudjit, L., Martins, P. M., Madjene, F., Petrovykh, D. Y., & Lanceros-Mendez, S. (2018). Photocatalytic reusable membranes for the effective degradation of tartrazine with a solar photoreactor. *Journal of Hazardous Materials*, *344*, 408–416. https://doi.org/10.1016/j.jhazmat.2017.10.053

Azalok, K. A., Oladipo, A. A., & Gazi, M. (2021). UV-light-induced photocatalytic performance of reusable MnFe-LDO–biochar for tetracycline removal in water. *Journal of Photochemistry and Photobiology A: Chemistry*, *405*(August), 112976. https://doi.org/10.1016/j.jphotochem.2020.112976

Baldrian, P., Verma, P., Stoytchev, I., & Stopka, P. (2004). *Degradation of BTEX and PAHs by Co (II) and Cu (II) -based radical-generating systems*. *51*, 159–164. https://doi.org/10.1016/j.apcatb.2004.02.011

Barbosa, C. A. S., Dias, P. M., Ferreira, A. M. da C., & Constantino, V. R. L. (2005). Mg-Al hydrotalcite-like compounds containing iron-phthalocyanine complex: Effect of aluminum substitution on the complex adsorption features and catalytic activity. *Applied Clay Science*, *28*(1-4 SPEC. ISS.), 147–158. https://doi.org/10.1016/j.clay.2004.02.002

Behbahani, E. S., Dashtian, K., & Ghaedi, M. (2021). Fe3O4-FeMoS4: Promise magnetite LDH-based adsorbent for simultaneous removal of Pb (II), Cd (II), and Cu (II) heavy metal ions. *Journal of Hazardous Materials*, *410*(November 2020), 124560. https://doi.org/10.1016/j.jhazmat.2020.124560

Bessaies, H., Iftekhar, S., Doshi, B., Kheriji, J., Ncibi, M. C., Srivastava, V., Sillanpää, M., & Hamrouni, B. (2020). Synthesis of novel adsorbent by intercalation of biopolymer in LDH for the removal of arsenic from synthetic and natural water. *Journal of Environmental Sciences (China)*, *91*(February), 246–261. https://doi.org/10.1016/j.jes.2020.01.028

Bini, M., Monteforte, F., Quinzeni, I., Friuli, V., Maggi, L., & Bruni, G. (2019). Hybrid compounds for improving drugs solubility: Synthesis, physico-chemical and pharmaceutical characterization of Nimesulide-LDH. *Journal of Solid State Chemistry*, *272*(January), 131–137. https://doi.org/10.1016/j.jssc.2019.02.001

Bokare, A. D., & Choi, W. (2014). Review of iron-free Fenton-like systems for activating H2O2 in advanced oxidation processes. In *Journal of Hazardous Materials* (Vol. 275). Elsevier B.V.

https://doi.org/10.1016/j.jhazmat.2014.04.054

Bouteraa, S., Saiah, F. B. D., Hamouda, S., & Bettahar, N. (2020). Zn-M-CO3 Layered Double Hydroxides (M=Fe, Cr, or Al): Synthesis, Characterization, and Removal of Aqueous Indigo Carmine. *Bulletin of Chemical Reaction Engineering & Catalysis*, *15*(1), 43–54. https://doi.org/10.9767/bcrec.15.1.5053.43-54

Britto, S., & Vishnu Kamath, P. (2009). Thermal, solution and reductive decomposition of Cu-Al layered double hydroxides into oxide products. *Journal of Solid State Chemistry*, *182*(5), 1193–1199. https://doi.org/10.1016/j.jssc.2009.02.003

Cavani, F., Trifirò, F., & Vaccari, A. (1991). Hydrotalcite-type anionic clays: Preparation, properties and applications. *Catalysis Today*, *11*(2), 173–301. https://doi.org/10.1016/0920-5861(91)80068-K

Chen, C., Li, Y., Ma, W., Guo, S., Wang, Q., & Li, Q. X. (2017). Mn-Fe-Mg-Ce loaded Al2O3 catalyzed ozonation for mineralization of refractory organic chemicals in petroleum refinery wastewater. *Separation and Purification Technology*, *183*, 1–10. https://doi.org/10.1016/j.seppur.2017.03.054

Cheng, M., Zeng, G., Huang, D., Lai, C., Xu, P., Zhang, C., & Liu, Y. (2016). Hydroxyl radicals based advanced oxidation processes (AOPs) for remediation of soils contaminated with organic compounds : A review. *Chemical Engineering Journal*, *284*, 582–598. https://doi.org/10.1016/j.cej.2015.09.001

Coelho, A., Castro, A. V, & Jr, G. L. S. A. (2006). *Treatment of petroleum refinery sourwater by advanced oxidation processes*. *137*, 178–184. https://doi.org/10.1016/j.jhazmat.2006.01.051

Dai, R., Liu, B., Zhang, Y., Pedersen, J. N., Zhang, X., Dong, M., & Guo, Z. (2021). Copper-based ternary hydrotalcite as a catalyst for hydroxylation of phenolic compounds. *Journal of Environmental Chemical Engineering*, *9*(6), 106390. https://doi.org/10.1016/j.jece.2021.106390

Dalanta, F., Kusworo, T. D., Aryanti, N., & Othman, N. H. (2021). Optimization of AC/TiO2/CeO2 composite formulation for petroleum refinery wastewater treatment via simultaneous adsorption-photocatalytic process using D-optimal mixture experimental design. *Journal of Environmental Chemical Engineering*, *9*(6), 106517. https://doi.org/10.1016/j.jece.2021.106517

Das, S., & Parida, K. (2021). Superior photocatalytic performance of Co Al LDH in the race of metal incorporated LDH: A comparison study. *Materials Today: Proceedings*, *35*, 275–280. https://doi.org/10.1016/j.matpr.2020.05.759

de Melo Costa-Serge, N., Gonçalves, R. G. L., Rojas-Mantilla, H. D., Santilli, C. V., Hammer, P., & Nogueira, R. F. P. (2021). Fenton-like degradation of sulfathiazole using copper-modified MgFe-CO3 layered double hydroxide. *Journal of Hazardous Materials*, *413*(October 2020). https://doi.org/10.1016/j.jhazmat.2021.125388

De Souza, G., Balzaretti, N. M., Marcílio, N. R., & Perez-Lopez, O. W. (2012). Decomposition of ethanol over Ni-Al catalysts: Effect of copper addition. *Procedia Engineering*, *42*(August), 335–345. https://doi.org/10.1016/j.proeng.2012.07.425

Demir-Duz, H., Ayyildiz, O., Aktürk, A. S., Álvarez, M. G., & Contreras, S. (2019). Approaching zero discharge concept in refineries by solar–assisted photo-Fenton and photo-catalysis processes. *Applied Catalysis B: Environmental*, *248*(September 2018), 341–348. https://doi.org/10.1016/j.apcatb.2019.02.026

Domingues, E., Quina, M. J., Quinta-ferreira, R. M., & Martins, R. C. (2018). *Detoxification of Olive Mill Wastewaters by Fenton ' s Process*. https://doi.org/10.3390/catal8120662

Domingues, E., Silva, M. J., Vaz, T., Gomes, J., & Martins, R. C. (2022). Science of the Total Environment Sulfate radical based advanced oxidation processes for agro-industrial ef fl uents treatment : A comparative review with Fenton ' s peroxidation. *Science of the Total Environment*, *832*(January), 155029.

https://doi.org/10.1016/j.scitotenv.2022.155029

Dubey, A., Rives, V., & Kannan, S. (2002). Catalytic hydroxylation of phenol over ternary hydrotalcites containing Cu, Ni and Al. *Journal of Molecular Catalysis A: Chemical*, *181*(1–2), 151–160. https://doi.org/10.1016/S1381-1169(01)00360-0

Dunn, T. (1989). MZAF: A BASIC program for off-line correction of electron microprobe data by the ZAF method. *Computers and Geosciences*, *15*(1), 9–17. https://doi.org/10.1016/0098-3004(89)90052-6

Ebrahimi, M., Kazemi, H., Mirbagheri, S. A., & Rockaway, T. D. (2016). An optimized biological approach for treatment of petroleum refinery wastewater. *Journal of Environmental Chemical Engineering*, *4*(3), 3401–3408. https://doi.org/10.1016/j.jece.2016.06.030

El-naas, M. H., Alhaija, M. A., & Al-zuhair, S. (2014). Journal of Environmental Chemical Engineering Evaluation of a three-step process for the treatment of petroleum refinery wastewater. *Biochemical Pharmacology*, *2*(1), 56–62. https://doi.org/10.1016/j.jece.2013.11.024

Eroi, S. N. gora., Ello, A. S., Diabaté, D., & Ossonon, D. B. (2021). Heterogeneous WO3/H2O2 system for degradationn of Indigo Carmin dye from aqueous solution. *South African Journal of Chemical Engineering*, *37*(April), 53–60. https://doi.org/10.1016/j.sajce.2021.03.009

Ferdous, S., Ioannidis, M. A., & Henneke, D. E. (2012). Effects of temperature, pH, and ionic strength on the adsorption of nanoparticles at liquid-liquid interfaces. *Journal of Nanoparticle Research*, *14*(5). https://doi.org/10.1007/s11051-012-0850-4

Frost, R. L., Ding, Z., Martens, W. N., Johnson, T. E., & Kloprogge, J. T. (2003). Molecular assembly in synthesised hydrotalcites of formula CuxZn6-xAl2(OH)16(CO3) · 4H2O - A vibrational spectroscopic study. *Spectrochimica Acta - Part A: Molecular and Biomolecular Spectroscopy*, *59*(2), 321–328. https://doi.org/10.1016/S1386-1425(02)00174-9

Fu, F., & Wang, Q. (2011). Removal of heavy metal ions from wastewaters: A review. *Journal of Environmental Management*, *92*(3), 407–418. https://doi.org/10.1016/j.jenvman.2010.11.011

Gallard, H., Laat, J. De, & Legube, B. (2019). *Revue des sciences de l ' eau Étude comparative de la vitesse de décomposition de H2O2 et de l ' atrazine par les systèmes Fe (III)/ H2O2 , Cu (II)/ H2O2 et Fe (III)/ Cu (II)/ H2O2 Comparative study of the rate of decomposition of H2O2 and of atra*. *Iii*.

Gallard, H., & Laat, J. D. E. (2000). *KINETIC MODELLING OF Fe (III)/ H 2 O 2 OXIDATION REACTIONS IN DILUTE AQUEOUS SOLUTION USING ATRAZINE AS A MODEL ORGANIC COMPOUND*. *34*(12), 3107–3116.

Gao, Z., Sasaki, K., & Qiu, X. (2018). Structural Memory Effect of Mg-Al and Zn-Al layered Double Hydroxides in the Presence of Different Natural Humic Acids: Process and Mechanism. *Langmuir*, *34*(19), 5386–5395. https://doi.org/10.1021/acs.langmuir.8b00059

Ghalehkhondabi, V., Fazlali, A., & Fallah, B. (2021). Performance analysis of four-stage rotating biological contactor in nitrification and COD removal from petroleum refinery wastewater. *Chemical Engineering and Processing - Process Intensification*, *159*(August 2020), 108214. https://doi.org/10.1016/j.cep.2020.108214

Gogate, P. R., & Pandit, A. B. (2004). *A review of imperative technologies for wastewater treatment I : oxidation technologies at ambient conditions*. *8*(03), 501–551. https://doi.org/10.1016/S1093-0191(03)00032-7

Guo, X., Ruan, Y., Diao, Z., Shih, K., Su, M., Song, G., Chen, D., Wang, S., & Kong, L. (2021). Environmental-friendly preparation of Ni–Co layered double hydroxide (LDH) hierarchical nanoarrays for efficient removing uranium (VI). *Journal of Cleaner Production*, *308*(May), 127384. https://doi.org/10.1016/j.jclepro.2021.127384

Guo, X. X., Hu, T. T., Meng, B., Sun, Y., & Han, Y. F. (2020). Catalytic degradation of anthraquinones-containing H2O2 production effluent over layered Co-Cu hydroxides: Defects facilitating hydroxyl radicals generation. *Applied Catalysis B: Environmental*, *260*(May 2019), 118157. https://doi.org/10.1016/j.apcatb.2019.118157

Haag, W. R., & David Yao, C. C. (1992). Rate Constants for Reaction of Hydroxyl Radicals with Several Drinking Water Contaminants. *Environmental Science and Technology*, *26*(5), 1005–1013. https://doi.org/10.1021/es00029a021

Hansen, É., Rodrigues, M. A. S., Aragão, M. E., & de Aquim, P. M. (2018). Water and wastewater minimization in a petrochemical industry through mathematical programming. *Journal of Cleaner Production*, *172*, 1814–1822. https://doi.org/10.1016/j.jclepro.2017.12.005

International Energy Agency. (2021). Oil 2021. *International Energy Agency*, 167. www.iea.org

Iqbal, M., Nisar, J., Adil, M., Abbas, M., Riaz, M., Tahir, M. A., Younus, M., & Shahid, M. (2017). Mutagenicity and cytotoxicity evaluation of photo-catalytically treated petroleum refinery wastewater using an array of bioassays. *Chemosphere*, *168*, 590–598. https://doi.org/10.1016/j.chemosphere.2016.11.021

Jain, M., Majumder, A., Ghosal, P. S., & Gupta, A. K. (2020). A review on treatment of petroleum refinery and petrochemical plant wastewater: A special emphasis on constructed wetlands. *Journal of Environmental Management*, *272*(June), 111057. https://doi.org/10.1016/j.jenvman.2020.111057

Johnston, A. L., Lester, E., Williams, O., & Gomes, R. L. (2021). Understanding Layered Double Hydroxide properties as sorbent materials for removing organic pollutants from environmental waters. *Journal of Environmental Chemical Engineering*, *9*(4), 105197. https://doi.org/10.1016/j.jece.2021.105197

Kameda, T., Uchida, H., Kumagai, S., Saito, Y., Mizushina, K., Itou, I., Han, T., & Yoshioka, T. (2021). Regeneration of carbonate-intercalated Mg–Al layered double hydroxides (CO3·Mg–Al LDHs) by CO2-induced desorption of anions (X) from X·Mg–Al LDH (X = Cl, SO4, or NO3): A kinetic study. *Chemical Engineering Research and Design*, *165*(2), 207–213. https://doi.org/10.1016/j.cherd.2020.10.032

Kannan, S., Dubey, A., & Knozinger, H. (2005). Synthesis and characterization of CuMgAl ternary hydrotalcites as catalysts for the hydroxylation of phenol. *Journal of Catalysis*, *231*(2), 381–392. https://doi.org/10.1016/j.jcat.2005.01.032

Karthikeyan, S., Priya, M. E., Boopathy, R., Velan, M., Mandal, A. B., & Sekaran, G. (2012). Heterocatalytic Fenton oxidation process for the treatment of tannery effluent: Kinetic and thermodynamic studies. *Environmental Science and Pollution Research*, *19*(5), 1828–1840. https://doi.org/10.1007/s11356-011-0691-1

KEFIF, F., EZZIANE, K., BAHMANI, A., BETTAHAR, N., & MAYOUF, S. (2019). Evans Blue dye removal from contaminated water on calcined and uncalcined $$\hbox {Cu-Al-CO}_{3}$$ Cu-Al-CO 3 layered double hydroxide materials prepared by coprecipitation. *Bulletin of Materials Science*, *42*(1), 14. https://doi.org/10.1007/s12034-018-1694-z

Kloprogge, J. T., & Frost, R. L. (1999). Infrared emission spectroscopic study of the thermal transformation of Mg-, Ni- and Co-hydrotalcite catalysts. *Applied Catalysis A: General*, *184*(1), 61–71. https://doi.org/10.1016/s0926-860x(99)00084-8

Lam, F. L. Y., & Hu, X. (2013). PH-insensitive bimetallic catalyst for the abatement of dye pollutants by photo-fenton oxidation. *Industrial and Engineering Chemistry Research*, *52*(20), 6639–6646. https://doi.org/10.1021/ie302864e

Lam, H., Chu, W., & Xu, W. (2021). Journal of Environmental Chemical Engineering Photocatalysis of naphthalene by Fe 3 O 4 / Oxone / UV : Simultaneous radical and non-radical pathways. *Journal of Environmental Chemical Engineering*, *9*(2), 105076. https://doi.org/10.1016/j.jece.2021.105076

Lebron, Y. A. R., Moreira, V. R., da Costa, P. R., Alkmin, A. R., de França Neta, L. S., Cerqueira, A. C., & Amaral, M. C. S. (2021). Chemical cleaning procedures on permeability recovery and lifespan of MBR membranes treating petroleum refinery wastewater: From bench- to pilot-scale applications. *Journal of Water Process Engineering*, *44*(November), 102411. https://doi.org/10.1016/j.jwpe.2021.102411

Li, C., Li, J., Wang, N., Zhao, Q., & Wang, P. (2021). Status of the treatment of produced water containing polymer in oilfields: A review. *Journal of Environmental Chemical Engineering*, *9*(4), 105303. https://doi.org/10.1016/j.jece.2021.105303

Liu, J., Wu, P., Li, S., Chen, M., Cai, W., Zou, D., Zhu, N., & Dang, Z. (2019). Synergistic deep removal of As(III) and Cd(II) by a calcined multifunctional MgZnFe-CO3 layered double hydroxide: Photooxidation, precipitation and adsorption. *Chemosphere*, *225*, 115–125. https://doi.org/10.1016/j.chemosphere.2019.03.009

Liu, Y., Cheng, M., Liu, Z., Zeng, G., Zhong, H., Chen, M., Zhou, C., Xiong, W., Shao, B., & Song, B. (2019). Heterogeneous Fenton-like catalyst for treatment of rhamnolipid-solubilized hexadecane wastewater. *Chemosphere*, *236*, 124387. https://doi.org/10.1016/j.chemosphere.2019.124387

Loganathan, S., Valapa, R. B., Mishra, R. K., Pugazhenthi, G., & Thomas, S. (2017). Thermogravimetric Analysis for Characterization of Nanomaterials. In *Thermal and Rheological Measurement Techniques for Nanomaterials Characterization* (Vol. 3). Elsevier Inc. https://doi.org/10.1016/B978-0-323-46139-9.00004-9

López, T., Bosch, P., Asomoza, M., Gómez, R., & Ramos, E. (1997). DTA-TGA and FTIR spectroscopies of sol-gel hydrotalcites: Aluminum source effect on physicochemical properties. *Materials Letters*, *31*(3–6), 311–316. https://doi.org/10.1016/S0167-577X(96)00296-0

Luo, H., Cheng, Y., Zeng, Y., Luo, K., & Pan, X. (2020). Enhanced decomposition of H2O2 by molybdenum disulfide in a Fenton-like process for abatement of organic micropollutants. *Science of the Total Environment*, *732*, 139335. https://doi.org/10.1016/j.scitotenv.2020.139335

Mak Yu, T., Caroline Reis Meira, A., Cristina Kreutz, J., Effting, L., Mello Giona, R., Gervasoni, R., Amado de Moura, A., Maestá Bezerra, F., & Bail, A. (2019). Exploring the surface reactivity of the magnetic layered double hydroxide lithium-aluminum: An alternative material for sorption and catalytic purposes. *Applied Surface Science*, *467–468*(July 2018), 1195–1203. https://doi.org/10.1016/j.apsusc.2018.10.221

Malato, S., Fernández-Ibáñez, P., Maldonado, M. I., Blanco, J., & Gernjak, W. (2009). Decontamination and disinfection of water by solar photocatalysis: Recent overview and trends. *Catalysis Today*, *147*(1), 1–59. https://doi.org/10.1016/j.cattod.2009.06.018

Mallakpour, S., & Khadem, E. (2017). Applications of biodegradable polymer/layered double hydroxide nanocomposites: Current status and recent prospects. In *Biodegradable and Biocompatible Polymer Composites: Processing, Properties and Applications*. Elsevier Ltd. https://doi.org/10.1016/B978-0-08-100970-3.00009-2

Mathematics, A. (2022). *Integral Method Solution of Time-Dependent Strained Diffusion-Reaction Layers with Multistep Kinetics Author (s): Werner J . A . Dahm , Gretar Tryggvason and Mei Zhuang Source : SIAM Journal on Applied Mathematics , Vol . 56 , No . 4 (Aug ., 1996), pp*. *56*(4), 1039–1059.

Mohanakrishna, G., Abu-Reesh, I. M., & Al-Raoush, R. I. (2018). Biological anodic oxidation and cathodic reduction reactions for improved bioelectrochemical treatment of petroleum refinery wastewater. *Journal of Cleaner Production*, *190*, 44–52. https://doi.org/10.1016/j.jclepro.2018.04.141

Mohapatra Lagnamayee, P. K. M. (2014). *A Review on Recent Progress, Challenges and Perspective of Layered Double Hydroxides as Promising Photocatalysts*.

Molaei, S., Moussavi, G., Talebbeydokhti, N., & Shekoohiyan, S. (2022). Biodegradation of the petroleum hydrocarbons using an anoxic packed-bed biofilm reactor with in-situ biosurfactant-producing bacteria. *Journal of Hazardous Materials*, *421*(July 2021), 126699. https://doi.org/10.1016/j.jhazmat.2021.126699

Naffrechoux, E., Chanoux, S., Petrier, C., & Suptil, J. (2000). Sonochemical and photochemical oxidation of organic matter. *Ultrasonics Sonochemistry*, *7*(4), 255–259. https://doi.org/10.1016/S1350-4177(00)00054-7

Nava-Andrade, K., Carbajal-Arízaga, G. G., Obregón, S., & Rodríguez-González, V. (2021). Layered double hydroxides and related hybrid materials for removal of pharmaceutical pollutants from water. *Journal of Environmental Management*, *288*(December 2020). https://doi.org/10.1016/j.jenvman.2021.112399

Navalon, S., Alvaro, M., & Garcia, H. (2010). Heterogeneous Fenton catalysts based on clays, silicas and zeolites. *Applied Catalysis B: Environmental*, *99*(1–2), 1–26. https://doi.org/10.1016/j.apcatb.2010.07.006

Nichela, D. A., Berkovic, A. M., Costante, M. R., Juliarena, M. P., & García Einschlag, F. S. (2013). Nitrobenzene degradation in Fenton-like systems using Cu(II) as catalyst. Comparison between Cu(II)- and Fe(III)-based systems. *Chemical Engineering Journal*, *228*, 1148–1157. https://doi.org/10.1016/j.cej.2013.05.002

Oladipo, A. A. (2021). CuCr2O4@CaFe–LDO photocatalyst for remarkable removal of COD from high-strength olive mill wastewater. *Journal of Colloid and Interface Science*, *591*, 193–202. https://doi.org/10.1016/j.jcis.2021.01.080

Oladipo, A. A., Ifebajo, A. O., & Gazi, M. (2019). Magnetic LDH-based CoO–NiFe2O4 catalyst with enhanced performance and recyclability for efficient decolorization of azo dye via Fenton-like reactions. *Applied Catalysis B: Environmental*, *243*, 243–252. https://doi.org/10.1016/j.apcatb.2018.10.050

Oller, I., Malato, S., & Sánchez-Pérez, J. A. (2011). Combination of Advanced Oxidation Processes and biological treatments for wastewater decontamination-A review. *Science of the Total Environment*, *409*(20), 4141–4166. https://doi.org/10.1016/j.scitotenv.2010.08.061

Palacio, L. A., Velásquez, J., Echavarría, A., Faro, A., Ribeiro, F. R., & Ribeiro, M. F. (2010). Total oxidation of toluene over calcined trimetallic hydrotalcites type catalysts. *Journal of Hazardous Materials*, *177*(1–3), 407–413. https://doi.org/10.1016/j.jhazmat.2009.12.048

Park, S., Baker, J. O., Himmel, M. E., Parilla, P. A., & Johnson, D. K. (2010). *Park2010.Pdf*. 1–10.

Patel, K., & Patel, M. (2020). Improving bioremediation process of petroleum wastewater using biosurfactants producing Stenotrophomonas sp. S1VKR-26 and assessment of phytotoxicity. *Bioresource Technology*, *315*(July), 123861. https://doi.org/10.1016/j.biortech.2020.123861

Pourehie, O., & Saien, J. (2020). Homogeneous solar Fenton and alternative processes in a pilot-scale rotatable reactor for the treatment of petroleum refinery wastewater. *Process Safety and Environmental Protection*, *135*, 236–243. https://doi.org/10.1016/j.psep.2020.01.006

Pradhan, A. C., Nanda, B., Parida, K. M., & Das, M. (2013). Quick photo-Fenton degradation of phenolic compounds by Cu/Al 2O3-MCM-41 under visible light irradiation: Small particle size, stabilization of copper, easy reducibility of Cu and visible light active material. *Dalton Transactions*, *42*(2), 558–566. https://doi.org/10.1039/c2dt32050a

Prado, C., Oliveira, M. De, Machado, M., Cristina, M., & Amaral, S. (2020). Journal of Water Process Engineering Coupling photocatalytic degradation using a green TiO 2 catalyst to membrane bioreactor for petroleum re fi nery wastewater reclamation. *Journal of Water Process Engineering*, *34*(December 2019), 101093. https://doi.org/10.1016/j.jwpe.2019.101093

Priyanka, Subbaramaiah, V., Srivastava, V. C., & Mall, I. D. (2014). Catalytic oxidation of nitrobenzene by copper loaded activated carbon. *Separation and Purification Technology*, *125*, 284–290. https://doi.org/10.1016/j.seppur.2014.01.045

Qiao, Z., Wang, Z., Zhang, C., Yuan, S., Zhu, Y., & Wang, J. (2012). PVAm–PIP/PS composite membrane with high

performance for CO_2/N_2 separation. *AIChE Journal*, *59*(4), 215–228. https://doi.org/10.1002/aic

Rajasekhar Pullabhotla, V. S. R., Southway, C., & Jonnalagadda, S. B. (2008). Ozone initiated oxidation of hexadecane with metal loaded γ-Al 2O3 catalysts. *Catalysis Letters*, *124*(1–2), 118–126. https://doi.org/10.1007/s10562-008-9434-4

Rezak, N., Bahmani, A., & Bettahar, N. (2021). Adsorptive removal of P(V) and Cr(VI) by calcined Zn-Al-Fe ternary LDHs. *Water Science and Technology*, *83*(10), 2504–2517. https://doi.org/10.2166/wst.2021.123

Rives, V., Dubey, A., & Kannan, S. (2001). Synthesis, characterization and catalytic hydroxylation of phenol over CuCoAl ternary hydrotalcites. *Physical Chemistry Chemical Physics*, *3*(21), 4826–4836. https://doi.org/10.1039/b103656b

Rives, V., Prieto, O., Dubey, A., & Kannan, S. (2003). Synergistic effect in the hydroxylation of phenol over CoNiAl ternary hydrotalcites. *Journal of Catalysis*, *220*(1), 161–171. https://doi.org/10.1016/S0021-9517(03)00245-8

Sá, F. P. De, Cunha, B. N., & Nunes, L. M. (2013). Effect of pH on the adsorption of Sunset Yellow FCF food dye into a layered. *Chemical Engineering Journal*, *215–216*, 122–127. https://doi.org/10.1016/j.cej.2012.11.024

Santo, C. E., Vilar, V. J. P., Botelho, C. M. S., Bhatnagar, A., Kumar, E., & Boaventura, R. A. R. (2012). Optimization of coagulation-flocculation and flotation parameters for the treatment of a petroleum refinery effluent from a Portuguese plant. *Chemical Engineering Journal*, *183*, 117–123. https://doi.org/10.1016/j.cej.2011.12.041

Santos, F. V., Azevedo, E. B., Sant'Anna, G. L., & Dezotti, M. (2006). Photocatalysis as a tertiary treatment for petroleum refinery wastewaters. *Brazilian Journal of Chemical Engineering*, *23*(4), 451–460. https://doi.org/10.1590/S0104-66322006000400003

Sing, K. S. W., & Williams, R. T. (2004). Physisorption hysteresis loops and the characterization of nanoporous materials. *Adsorption Science and Technology*, *22*(10), 773–782. https://doi.org/10.1260/0263617053499032

Singh, B., & Kumar, P. (2020). Pre-treatment of petroleum refinery wastewater by coagulation and flocculation using mixed coagulant: Optimization of process parameters using response surface methodology (RSM). *Journal of Water Process Engineering*, *36*(February), 101317. https://doi.org/10.1016/j.jwpe.2020.101317

Sun, Y., Zhang, Y., & Quan, X. (2008). Treatment of petroleum refinery wastewater by microwave-assisted catalytic wet air oxidation under low temperature and low pressure. *Separation and Purification Technology*, *62*(3), 565–570. https://doi.org/10.1016/j.seppur.2008.02.027

Taylor, P., Tony, M. A., Purcell, P. J., & Zhao, Y. (n.d.). *Journal of Environmental Science and Health , Part A : Toxic / Hazardous Substances and Environmental Oil refinery wastewater treatment using physicochemical , Fenton and Photo-Fenton oxidation processes Oil refinery wastewater treatment using physicochem*. *November 2014*, 37–41. https://doi.org/10.1080/10934529.2012.646136

Ulhaq, I., Ahmad, W., Ahmad, I., Yaseen, M., & Ilyas, M. (2021). Engineering TiO2 supported CTAB modified bentonite for treatment of refinery wastewater through simultaneous photocatalytic oxidation and adsorption. *Journal of Water Process Engineering*, *43*(July), 102239. https://doi.org/10.1016/j.jwpe.2021.102239

Valeikiene, L., Roshchina, M., Grigoraviciute-Puroniene, I., Prozorovich, V., Zarkov, A., Ivanets, A., & Kareiva, A. (2020). On the reconstruction peculiarities of sol–gel derived mg2−xmx/al1 (M = ca, sr, ba) layered double hydroxides. *Crystals*, *10*(6), 1–19. https://doi.org/10.3390/cryst10060470

Valente, J. S., Rodriguez-Gattorno, G., Valle-Orta, M., & Torres-Garcia, E. (2012). Thermal decomposition kinetics of MgAl layered double hydroxides. *Materials Chemistry and Physics*, *133*(2–3), 621–629. https://doi.org/10.1016/j.matchemphys.2012.01.026

Vendramel, S., Bassin, J. P., Dezotti, M., & Sant'Anna, G. L. (2015). Treatment of petroleum refinery wastewater

containing heavily polluting substances in an aerobic submerged fixed-bed reactor. *Environmental Technology (United Kingdom)*, *36*(16), 2052–2059. https://doi.org/10.1080/09593330.2015.1019933

Wang, Hao, Jing, M., Wu, Y., Chen, W., & Ran, Y. (2018b). Effective degradation of phenol via Fenton reaction over CuNiFe layered double hydroxides. *Journal of Hazardous Materials*, *353*(September 2017), 53–61. https://doi.org/10.1016/j.jhazmat.2018.03.053

Wang, Hao, Zhang, Z., Jing, M., Tang, S., Wu, Y., & Liu, W. (2020b). Synthesis of CuNiSn LDHs as highly efficient Fenton catalysts for degradation of phenol. *Applied Clay Science*, *186*(December 2019), 105433. https://doi.org/10.1016/j.clay.2019.105433

Wang, Hui, Xiang, X., Li, F., Evans, D. G., & Duan, X. (2009). Investigation of the structure and surface characteristics of Cu-Ni-M(III) mixed oxides (M = Al, Cr and In) prepared from layered double hydroxide precursors. *Applied Surface Science*, *255*(15), 6945–6952. https://doi.org/10.1016/j.apsusc.2009.03.019

Wang, N., Sun, X., Zhao, Q., & Wang, P. (2021). Treatment of polymer-flooding wastewater by a modified coal fly ash-catalysed Fenton-like process with microwave pre-enhancement: System parameters, kinetics, and proposed mechanism. *Chemical Engineering Journal*, *406*(May 2020), 126734. https://doi.org/10.1016/j.cej.2020.126734

Wang, N., Zheng, T., Zhang, G., & Wang, P. (2015). *A review on Fenton-like processes for organic wastewater treatment*. https://doi.org/10.1016/j.jece.2015.12.016

Wang, X., Lin, Y., Su, Y., Zhang, B., Li, C., Wang, H., & Wang, L. (2017). Design and synthesis of ternary-component layered double hydroxides for high-performance supercapacitors: understanding the role of trivalent metal ions. *Electrochimica Acta*, *225*, 263–271. https://doi.org/10.1016/j.electacta.2016.12.160

Wang, X., Wang, Z., Yin, X., Zhao, H., Wu, C., & Liu, X. (2021). Promotion of NO oxidation through H2O2 thermal decomposition using a metal surface. *Process Safety and Environmental Protection*, *152*, 455–461. https://doi.org/10.1016/j.psep.2021.06.037

Wang, Y., Zhao, H., & Zhao, G. (2015). Iron-copper bimetallic nanoparticles embedded within ordered mesoporous carbon as effective and stable heterogeneous Fenton catalyst for the degradation of organic contaminants. *Applied Catalysis B: Environmental*, *164*, 396–406. https://doi.org/10.1016/j.apcatb.2014.09.047

Wu, K., Xu, S., Tian, X. Y., Zeng, H. Y., Hu, J., Guo, Y. H., & Jian, J. (2021). Renewable lignin-based surfactant modified layered double hydroxide and its application in polypropylene as flame retardant and smoke suppression. *International Journal of Biological Macromolecules*, *178*, 580–590. https://doi.org/10.1016/j.ijbiomac.2021.02.148

Xie, Z.-H., Zhou, H.-Y., He, C.-S., Pan, Z.-C., Yao, G., & Lai, B. (2021). Synthesis, application and catalytic performance of layered double hydroxide based catalysts in advanced oxidation processes for wastewater decontamination: A review. *Chemical Engineering Journal*, *414*(October 2020), 128713. https://doi.org/10.1016/j.cej.2021.128713

Xie, Z., Zhou, J., Wang, J., François-Xavier, C. P., & Wintgens, T. (2019). Novel Fenton-like catalyst Γ-Cu-Al2O3-Bi12O15Cl6 with electron-poor Cu centre and electron-rich Bi centre for enhancement of phenolic compounds degradation and H2O2 utilization: The synergistic effects of Σ-Cu-ligand, dual-reaction centres and oxygen vaca. *Applied Catalysis B: Environmental*, *253*(January), 28–40. https://doi.org/10.1016/j.apcatb.2019.04.032

Yadav, B. S., & Dasgupta, S. (2022). Effect of time, pH, and temperature on kinetics for adsorption of methyl orange dye into the modified nitrate intercalated MgAl LDH adsorbent. *Inorganic Chemistry Communications*, *137*(September 2021), 109203. https://doi.org/10.1016/j.inoche.2022.109203

Yang, C., Liao, L., Lv, G., Wu, L., Mei, L., & Li, Z. (2016). Synthesis and characterization of Mn intercalated Mg-Al hydrotalcite. *Journal of Colloid and Interface Science*, *479*, 115–120. https://doi.org/10.1016/j.jcis.2016.06.057

Yang, J., Huang, R., Cao, Y., Wang, H., Ivanets, A., & Wang, C. (2022). Heterogeneous Fenton degradation of persistent organic pollutants using natural chalcopyrite: effect of water matrix and catalytic mechanism. *Environmental Science and Pollution Research*, *0123456789*. https://doi.org/10.1007/s11356-022-21105-0

Yang, Y., Du, X., Abudula, A., Zhang, Z., Ma, X., Tang, K., Hao, X., & Guan, G. (2019). Highly efficient defluoridation using a porous MWCNT@NiMn-LDH composites based on ion transport of EDL coupled with ligand exchange mechanism. *Separation and Purification Technology*, *223*(December 2018), 154–161. https://doi.org/10.1016/j.seppur.2019.04.052

Zaviska, F., Drogui, P., Mercier, G., & Blais, J. F. (2009). Advanced oxidation processes for waters and wastewaters treatment: Application to degradation of refractory pollutants. *Revue Des Sciences de l'Eau*, *22*(4), 535–564. https://doi.org/10.7202/038330ar

Zhang, P., Ouyang, S., Li, P., Gu, Z., Huang, Y., & Deng, S. (2019). Effect of anion co-existence on ionic organic pollutants removal over Ca based layered double hydroxide. *Journal of Colloid and Interface Science*, *534*, 440–446. https://doi.org/10.1016/j.jcis.2018.09.019

Zhou, S., Qian, Z., Sun, T., Xu, J., & Xia, C. (2011a). Catalytic wet peroxide oxidation of phenol over Cu-Ni-Al hydrotalcite. *Applied Clay Science*, *53*(4), 627–633. https://doi.org/10.1016/j.clay.2011.05.013

Zhu, K., Liu, C., Ye, X., & Wu, Y. (1998). *Catalysis of hydrotalcite-like compounds in liquid phase oxidation : (I) phenol hydroxylation*. *168*.

Declaration of interests

☒The authors declare that they have no known competing financial interests or personal relationships that could have appeared to influence the work reported in this paper.

☐The authors declare the following financial interests/personal relationships which may be considered as potential competing interests: